Global and Planetary Change 229 (2023) 104237

Contents lists available at ScienceDirect

Global and Planetary Change

journal homepage: www.elsevier.com/locate/gloplacha

Widespread cooling over West Antarctica and adjacent seas over the past millennium

Zhiqiang Lyu [a,b,*], Hugues Goosse [a], Quentin Dalaiden [a], Xavier Crosta [c], Johan Etourneau [c,d]

[a] Earth and Life Institute, UCLouvain, Louvain-la-Neuve, Belgium
[b] Department of Atmospheric and Environmental Sciences, University at Albany, Albany, NY 12226, USA
[c] Université de Bordeaux, CNRS, UMR 5805 EPOC, 33615 Pessac Cedex, France
[d] Ecole Pratique des Hautes Etudes, PSL Research University, 75014 Paris, France

ARTICLE INFO

Editor: Dr. Alan Haywood

Keywords:
West Antarctica
Past millennium
Centennial-scale temperature changes
Volcanic forcing

ABSTRACT

Instrumental observations have highlighted strong interconnections within the Antarctic climate system between atmosphere, ocean and sea ice over the past few decades. Our goal in this study is to leverage these links by combining marine and terrestrial records with climate modeling results, using data assimilation, to reconstruct past climate changes in West Antarctica and the surrounding seas. Through comparing two data assimilation experiments that use the same terrestrial proxy records with annual and decadal temporal resolutions, we confirm that the covariance relationship between several key climate variables (surface air temperature (SAT), sea ice, and atmospheric circulation), used in the data assimilation is time scale dependent. Our experiments show that a data assimilation step of 10 years appears to be a good compromise. Additionally, we clarify the contributions of continental and marine records to the reconstructions through two separate data assimilation experiments: one using the continental proxies only and another using both continental and marine records. Our results suggest that the latter is more useful, providing a stronger and more direct constraint on the evolution of the ocean-atmosphere coupled system, and is more reliable, as suggested by the validation against independent sea ice-related marine records. Based on our reconstruction for multiple variables covering the past two millennia, we confirmed a widespread cooling trend occurred over West Antarctica and surrounding seas over the period 900–1800 CE. This reconciles the inconsistency between some existing reconstructions and climate model results, in particular over the Antarctic Peninsula. This cooling could be explained by a direct thermodynamic response to external forcing, with a dominant contribution of the volcanic forcing over the period. Our results thus highlight that West Antarctica and surrounding seas are sensitive to external forcings at this time scale and that the temperature evolution there is coherent with global changes at the centennial scale over the past millennium.

1. Introduction

Over the past decades, the West Antarctic climate has experienced pronounced interannual and decadal variations, with a remarkable warming that is two times faster than the global average from the 1970s to the 1990s followed by a pause or a cooling in the first two decades of the 21st century (Turner et al., 2016; Turner et al., 2020; Steig et al., 2009). Many studies have attributed this change to the combined effects of the depleted stratospheric ozone, increased greenhouse gas concentrations (Thompson and Solomon, 2002; Marshall et al., 2004) and internal variability, in particular related to tropical-high-latitude atmospheric teleconnections (Ding et al., 2011; Clem et al., 2020; Li et al., 2021), and atmospheric-sea ice interactions (Turner et al., 2016). However, the short length of the instrumental records limits our ability to fully estimate the contribution of the respective forcings compared with the internal variability, especially at decadal to centennial scales (Jones et al., 2016; Clem et al., 2020).

Studying climate variability over the past millennia offers the possibility to gain insight into decadal- to centennial-scale changes that cannot be discerned from instrumental data. To this end, SAT for West Antarctica has been reconstructed from proxy data, mainly using borehole temperature (e.g., Orsi et al., 2012), water isotopic records from ice cores (e.g., Stenni et al., 2017), and climate model simulations (e.g., Klein et al., 2019). Nevertheless, clear differences have been obtained

* Corresponding author at: Earth and Life Institute, UCLouvain, Louvain-la-Neuve, Belgium.
E-mail addresses: zhiqiang.lyu@student.uclouvain.be, zlyu2@albany.edu (Z. Lyu).

https://doi.org/10.1016/j.gloplacha.2023.104237
Received 28 November 2022; Received in revised form 2 September 2023; Accepted 4 September 2023
Available online 6 September 2023

between the various proxy-based reconstructions, as well as between reconstructions and modeling results. As a consequence, the past SAT changes over West Antarctica are still relatively uncertain, especially the magnitude of a potential multi-centennial cooling trend over the past millennium that is sometimes referred to as the transition from a relatively mild Medieval Climate Anomaly (MCA) to a colder Little Ice Age (LIA), identified in some regions of the Northern Hemisphere (Bradley et al., 2003; Mann et al., 2009).

Among all existing proxy-based temperature reconstructions, Stenni et al. (2017) presents probably the most extensive one. On the basis of 112 ice-core water isotopic records, they provide SAT reconstructions for seven Antarctic regions over the past two millennia, including two regions for West Antarctica: the Antarctic Peninsula (AP) and the West Antarctica Ice Sheet (WAIS). While a pronounced cooling over the past millennium is reconstructed for the WAIS, similar to many other regions of the world (PAGES 2k Consortium, 2013; McGregor et al., 2015), the trend is much weaker in the AP. However, the weak multi-centennial variability in the AP climate reconstructed by Stenni et al. (2017) seems inconsistent with the glacial advance that occurred from 1550 to 1860 CE (Simms et al., 2021). Additionally, Lüning et al. (2019) found that non-ice temperature sensitive records (mainly lake and marine sediments) suggest a generally warm MCA and cold LIA in the AP. The sea ice-related diatom records from marine sediments also suggest a heavier sea ice cover in the eastern AP since 1300 CE (Barbara et al., 2016). Finally, the simulations performed in the framework of the Past Model Intercomparison Project (PMIP3, Otto-Bliesner et al., 2009) and the fifth phase of the Coupled Model Intercomparison Project (CMIP5; Taylor et al., 2012) show a significant and widespread cooling over West Antarctica during the pre-industrial past millennium (Klein et al., 2019; Silvestri et al., 2021), which also disagrees with the reconstruction in Stenni et al. (2017) for the AP.

Studies based on reconstructions and model simulations have suggested that the solar and volcanic forcings are the main drivers of the cooling trend over West Antarctica during the past millennium (e.g., Orsi et al., 2012; Goosse et al., 2012). At the first order, the response to this forcing is expected to give a relatively homogenous cooling over the region due to reduced radiative forcing. However, large-scale modes of variability such as the Southern Annular mode (SAM, the primary pattern of climate variability in the extra-tropical Southern Hemisphere characterized by opposing pressure and temperature anomalies over the middle and high southern latitudes), or changes in the Amundsen Sea Low (ASL, a climatological low-pressure system centered in the Amundsen Sea) can also modulate the surface climate at multi-decadal time scales (Lyu et al., 2021; Dalaiden et al., 2021). For instance, the latter could induce temperature changes of different magnitude or even sign in West Antarctica, as a function of modifications of its location associated with changes in wind direction and intensity (e.g., Hosking et al., 2013; Dalaiden et al., 2021). Describing precisely the pattern of past temperature changes is thus essential to identify the relative contribution of a direct radiative forcing and of atmospheric circulation changes.

Within this framework, the goal of the present study is to investigate the potential existence of widespread cooling over West Antarctica and adjacent seas over the past millennium and to identify the underlying mechanisms. Our analysis is mainly based on the data assimilation (DA) method that combines observational data and model results to reconstruct the state of the climate system (e.g., Hakim et al., 2016). Previous offline DA-based reconstructions (Dalaiden et al., 2021; O'Connor et al., 2021) assimilate annually resolved continental data to obtain atmospheric states and oceanic conditions (in particular sea ice). However, the covariance between atmospheric and oceanic variables could be non-stationary across different time scales. For instance, the response of sea ice and oceanic temperatures in the Southern Ocean to stronger westerly winds includes a several-years long cooling and sea ice expansion due to the induced northward transport of cold Antarctic surface waters, potentially followed at the decadal scale by a warming due to the upwelling of Circumpolar Deep Water (Ferreira et al., 2015).

In contrast to previous studies, here we assimilate four alkenone-based sea surface temperature (SST) reconstructions off the southern Chilean coast and one diatom-based sea ice presence reconstruction off the coast of Adelie Land in the data assimilation experiments. Alkenones are organic compounds preserved in marine sediments that can be the basis for a robust biogeochemical proxy for estimating SSTs or very near-surface (upper mixed layer) ocean temperatures in paleoceanography. Diatoms are microscopic single-celled algae that inhabit a wide range of aquatic and sub-aquatic environments (e.g., Allen and Weich, 2022). Some diatoms (e.g., Fragilaropsis curta and Fragilaropsis cylindrus) that are known to be associated with sea ice have been applied to identify qualitatively specific sea ice conditions (e.g., Etourneau et al., 2013; Allen and Weich, 2022), and their relative abundance could link the quantitative sea-ice conditions using statistical methods (e.g., Barbara et al., 2016; Crosta et al., 2021). Compared to the continental proxy records with annual or nearly annual resolutions, marine proxy records retain in general lower-frequency signals because of their lower sedimentation rate. Therefore, assimilating them directly could give a stronger and more direct constraints on the different components of the ocean-atmosphere coupled system, and better investigate the evolution of slower components of the climate system.

2. Data and methods

2.1. Proxy records

For the continental proxy records with annual temporal resolution, we rely on ice-core based snow accumulation and water isotope ($\delta^{18}O$) data synthesized in Thomas et al. (2017) and Stenni et al. (2017). We selected records from West Antarctica that span the full (or almost full) Common Era (1–2000 CE) because we are interested in long-term changes and to avoid issues related to using differing numbers of records over time. This corresponds to five $\delta^{18}O$ records and two snow accumulation records ($\delta^{18}O$-DA and SN-DA, respectively, in Fig. 1). In addition to the continental proxy records, we use four well-constrained multi-decadal alkenone-based SST reconstructions off the southern Chilean coast (SST-DA in Fig. 1) and one quantitative reconstruction of sea ice presence off the coast of Adelie Land in Antarctica (SIP-DA in Fig. 1). They all cover the period 1–1800 CE. The selection of these oceanic records is based on several criteria. Firstly, they are sensitive to sea surface temperature and sea ice changes. Secondly, a reliable age model with at least two control points for each 200-year interval of the past millennium has been established for each record. Additionally, these records have a temporal resolution of no <50 years. Lastly, they are situated in the South Pacific sector (as shown in Fig. 1) which is geographically closest to our research area of interest, West Antarctica. Although the records in the southern coast of Chile may be situated north of the Southern Ocean frontal system and contain some localized signals, they provide useful information about Antarctica due to the teleconnections between the regions or common driving mechanisms. Previous studies argued that the alkenone-based SST reconstructions could have a small bias toward the summer blooming season (e.g., Tierney and Tingley, 2018). Therefore, we test the sensitivity of the DA-based reconstructions (ASSIM-P2000-DJF) to the seasonality of these SST reconstructions, as described in Section 3.2.

In addition, several marine diatom records in the AP and Ross Sea coast (SI-Valid in Fig. 1) are used to evaluate our results (see details in Section 3.2) as assimilating directly those qualitative records is difficult. Detailed information about these records is provided in Table 1. These records are carefully selected for the following reasons:

(1) Their geographic location aligns with the region of interest, ensuring relevance to our study.
(2) Previous studies, such as Barbara et al. (2016), Bárcena et al. (1998), Etourneau et al. (2013), Christ et al. (2015), and Mezgec

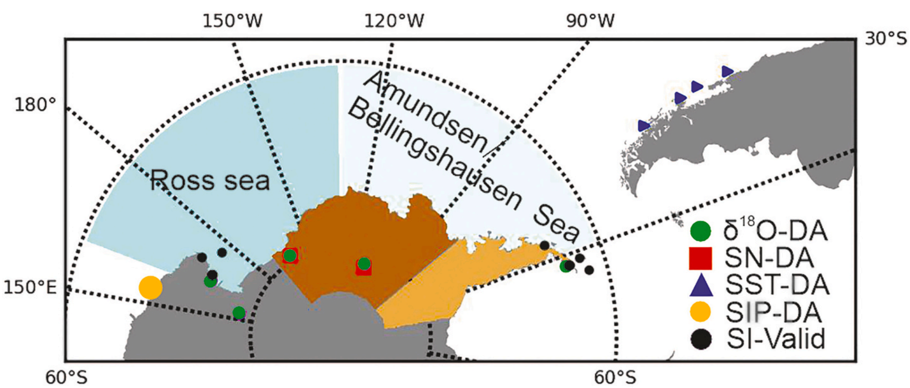

Fig. 1. Locations of the proxy records covering the past two millennia used in this study: four SST reconstructions (blue triangle, SST-DA), one reconstruction of sea ice persistence (yellow circle, SIP-DA), five precipitation-weighted $\delta^{18}O$ records (green circles, $\delta^{18}O$-DA) and two snow accumulation records (red rectangles, SN-DA). The black circles (SI-Valid) indicate the locations of the marine diatom data used for the qualitative validation of our results. The green shaded area in the Southern Ocean denotes two zones with regional-scaled sea ice extent (i.e., at least 15% of the ocean surface covered by sea ice) following the definition of Parkinson (2019): the Bellingshausen/Amundsen Sea zone (130°W-60°E, light green) and the Ross Sea zone (160°E-130°W, dark green). The brown shaded area in Antarctica represents two climate regions investigated in this study including the Antarctic Peninsula (AP, 70–74°S, 60°W - 80°W, light brown) and the West Antarctic Ice Sheet (WAIS, north of 85°S, 60°W-170°W, dark brown), as defined by Stenni et al. (2017). (For interpretation of the references to colour in this figure legend, the reader is referred to the web version of this article.)

Table 1
(a) Description of the proxy records covering the past two millennia used for the DA experiments. (b) Description of the sea-ice proxy records used for the validation.

(a) Name	Location	Proxy type	Reference
GeoB3313–1	Southern Chilean coast	Alkenone	Lamy et al., 2002
MD07–3093	Southern Chilean coast	Alkenone	Collins et al., 2019
MD07–3088	Southern Chilean coast	Alkenone	Haddam et al., 2018
MD07–3124	Southern Chilean coast	Alkenone	Caniupán et al., 2014
James Ross Island	Antarctic Peninsula	$\delta^{18}O$	Mulvaney et al., 2012
WDC06A	West Antarctic Ice Sheet	$\delta^{18}O$	Steig et al., 2013
RICE	West Antarctic Ice Sheet	$\delta^{18}O$	Bertler et al., 2018
Taylor Dome	Ross Sea coast	$\delta^{18}O$	Steig et al., 2000
TALDICE-Talos Dome	Ross Sea coast	$\delta^{18}O$	Stenni et al., 2011
RICE	West Antarctic Ice Sheet	Snow accumulation	Winstrup et al., 2019
WAIS 2014	West Antarctic Ice Sheet	Snow accumulation	Banta et al., 2008
IODP U1357B	Adelie Land coast	Marine diatom	Crosta et al., 2021
(b) Name	**Location**	**Proxy type**	**Reference**
GEBRA2	Antarctic Peninsula coast	Marine diatom	Bárcena et al., 1998
GEBRA1	Antarctic Peninsula coast	Marine diatom	Bárcena et al., 1998
A3	Antarctic Peninsula coast	Marine diatom	Bárcena et al., 2002
A6	Antarctic Peninsula coast	Marine diatom	Bárcena et al., 2002
JPC38	Antarctic Peninsula coast	Marine diatom	Barbara et al., 2016
JPC10	Antarctic Peninsula coast	Marine diatom	Etourneau et al., 2013
JPC127	Antarctic Peninsula coast	Marine diatom	Christ et al., 2015
ODP1098B	Antarctic Peninsula coast	TEX86	Shevenell et al., 2011
Wood Bay (WB)	Ross Sea coast	Marine diatom	Mezgec et al., 2017
Cape Hallett (CH)	Ross Sea coast	Marine diatom	Mezgec et al., 2017
Joides Basin (JB)	Ross Sea coast	Marine diatom	Mezgec et al., 2017

et al. (2017), have identified these records as being closely linked to sea ice changes. Therefore, they serve as reliable qualitative proxies for monitoring sea ice variations.

(3) We have included records that meet the criterion of having at least two age control points per 500-year interval and having established an age model using methods such as sedimentation rate. This ensures that we can effectively compare the proxy records with our reconstruction in a coherent time domain.

It remains a challenge for current paleoclimate DA techniques to integrate proxies with varying temporal resolutions (Steiger and Hakim, 2016). Therefore, in addition to the tests performed at annual resolution using only high-resolution records, we select a uniform timescale of 10 years to merge low-resolution marine records with high-resolution continental records. Specifically, we have applied a 10-year bin average for annually resolved continental proxies, while we have utilized linear interpolation to obtain a pseudo-decadal resolution for multi-decadal marine records.

We also assimilate another set of data for validation (these experiments are named ASSIM-P200-1 yr and ASSIM-P200-10 yr, see in Table 2), which is the same as that used in Dalaiden et al. (2021) and includes all ice-core based annually resolved records from the databases of Stenni et al. (2017) and Thomas et al. (2017), as well as tree-ring width records located in the Southern Hemisphere from the PAGES 2 K database. It should be noted that we have only used locations in WA,

Table 2
Description of the DA experiments.

Name	Assimilated proxy records	Temporal resolution	Temporal span
ASSIM-P200-1 yr	20 ice-core based $\delta^{18}O$ and 34 snow accumulation records in West Antarctica and 6 tree ring width records (Fig. S1)	1 year	1800–2000 CE
ASSIM-P200-10 yr	20 ice-core based $\delta^{18}O$ and 34 snow accumulation records in West Antarctica and 6 tree ring width records (Fig. S1)	10 years	1800–2000 CE
ASSIM-P2000-CON	Five ice-core based $\delta^{18}O$ and two snow accumulation records in West Antarctica (Fig. 1)	10 years	1–2000 CE
ASSIM-P2000-ALL	Five ice-core based $\delta^{18}O$ and two snow accumulation records in West Antarctica and four SST reconstructions (Fig. 1)	10 years	1–2000 CE
ASSIM-P2000-DJF	Same as ASSIM-P2000-ALL but assuming that SST reconstructions represent summer conditions	10 years	1–2000 CE

including 34 snow accumulation records and 20 $\delta^{18}O$ records shown in Fig. S1, in contrast to Dalaiden et al. (2021), who used ice-core data from all of Antarctica.

2.2. Climate model simulations

As in some recent studies (e.g., Dalaiden et al., 2021; O'Connor et al., 2021), three simulations performed with the isotope-enabled Community Earth System Model version 1 (iCESM1, Brady et al., 2019; Stevenson et al., 2019) are used here as prior modeling simulations. iCESM1 is a coupled atmosphere-ocean-sea ice model that includes atmosphere and land components with a $\sim 2^{\circ}$ resolution and an ocean component with a $\sim 1^{\circ}$ resolution. The transient simulations are run from 850 to 2005 CE driven by the estimated solar, volcanic, greenhouse gases, aerosols, land-use, and orbital forcings. Three simulations were given identical forcings but differed slightly in the initial atmospheric state; this difference was sufficient to generate simulations with different internal ocean-atmosphere variability and therefore different time trajectories (Brady et al., 2019). One of the main advantages of using an isotope-enabled model is the possibility to make a direct comparison with the proxy records. The modeling results have been fully evaluated for Antarctica. While some biases are present, in particular at a local scale, the simulations represent well the current climate from 1979 to 2005 CE for near-surface air temperature, snow accumulation, the mean state of Antarctic sea-ice extent, and geopotential height at 500-hPa, which are the variables investigated here (Dalaiden et al., 2021).

2.3. Particle-filter based offline data assimilation method

To estimate the state of the climate system, we apply an ensemble-based offline data assimilation approach, similar to many previous studies (e.g., Hakim et al., 2016; Steiger et al., 2018; Klein et al., 2019), using a particle filter method as described by Dubinkina et al. (2011). The ensemble of model states is derived from three simulations performed with iCESM1 for the period 850–1850 CE. Two different temporal assimilation windows of 1-year and 10 years are applied in the DA experiments, providing ensembles with 3003 (=1001 × 3) and 300 (= 100 × 3) members or particles, respectively, referred to as prior distributions. For a specific year or decade, each particle in the ensemble is compared with the data to determine its likelihood for this period, taking the data uncertainty into account. Particles with high similarity to the data receive a higher weight, while those with large differences from observations receive a lower weight. When the weight of each particle for that given year or decade is obtained, a weighted mean of the model states is calculated and provided as the mean reconstruction. The uncertainty of the DA-based reconstruction can then be given by the standard deviation of the weighted ensemble. Relying on the covariance relationship between climatic variables as represented in the prior model, information from where the constraints apply can be propagated to any other simulated variables, even those not directly constrained by the proxy data. This means that our reconstruction provides all the physical variables simulated by the model. Here, the variables we analyze are sea ice concentration, sea level pressure, SAT, and subsurface sea temperature at 100 m and 500 m as they are key to understand the processes at play. In our analyses, the SAM index is defined as the normalized difference in mean sea-level pressure between 40° and 65° bands (Gong and Wang, 1999). The ASL index is defined as the normalized mean of the sea level pressure from 75°S to 60°S and 170°E to 70°W (Fogt et al., 2012; Hosking et al., 2013). For the regional-scale sea ice extent (i.e., at least 15% of the ocean surface covered by ice, Fig. 1), we follow the geographical definition of Parkinson (2019) and divide the ocean off West Antarctica into two zones: the Bellingshausen/Amundsen Sea zone (130°W-60°E) and the Ross Sea zone (160°E-130°W). The definition of the climate regions (Fig. 1), i.e., the AP (70–74°S, 60°W - 80°W) and the WAIS (north of 85°S, 60°W-170°W), follows those in Stenni et al. (2017).

The comparison between the modeling results and continental proxy records is based on a coarser spatial grid than the initial modeling grid to reduce the effect of the model's inability to reproduce local features and small-scale noise in the records. To achieve this, we follow the same approach as Dalaiden et al. (2021) by computing composites that include all records located within 500 km × 500 km cells and linearly interpolating the initial prior modeling grid onto the 500 km regular grid. For the snow accumulation records, each original time series is first normalized for the period 1941–1990 CE and then calibrated to have the same mean and variance as the snow accumulation reconstruction of Medley and Thomas (2019) for the same boxes over the same period. The $\delta^{18}O$ composite for each grid cell is calculated by averaging the anomalies of $\delta^{18}O$ records over the period 1941–1990 CE. This period matches the period used to compute the SMB (surface mass balance) anomalies in order to keep coherence between both. The calculation of the $\delta^{18}O$ composite does not require initial normalization because of its lesser dependence on spatial distribution compared to the snow accumulation records.

Estimation of the data error is a crucial step in data assimilation since errors determine the strength of the constraint provided by each proxy record. In this study, we adopt the method of Dalaiden et al. (2021) to define the error for the ice-core-based $\delta^{18}O$ and snow accumulation. Despite the spatial averaging of records over 500 km × 500 km cells, ice core composites preserve climatic information at spatial scales smaller than the spatial resolution of iCESM1. A large fraction of the observation error for the $\delta^{18}O$ or snow accumulation composites could thus arise from their spatial representativeness. To evaluate the magnitude of this term, we use a simulation with a high spatial resolution of 27 km performed using the latest version of the polar-oriented Regional Atmospheric Climate MOdel (RACMO2.3p2, hereafter RACMO) (Van Wessem et al., 2018). We calculate the standard deviation of the differences between the average of the annual mean snow accumulation time series using only the original RACMO grid cell (~27 km) where ice core records are available and the "true" average over the continental part of 500 km cells. This standard deviation is then used as the error of the snow accumulation records. The same method is used to calculate the error in the $\delta^{18}O$ records. Since no physical variable with water isotope is generated by RACMO, a finer model is obtained by linear interpolation of iCESM1 to the RACMO grid for the period 1950–2005. For the error of the 10-year averaged data, we account for the smoothing of the time series by dividing the error given at the interannual scale mentioned above by a factor of $\sqrt{10}$ (as is commonly done, for instance, in PAGES 2k-PMIP3 group, 2015).

We selected a relatively low value of 0.5 °C for the error of SST reconstructions, and we do not consider the uncertainties in age models for marine records, corresponding to an underestimation of the total uncertainties that likely affect the robustness of our reconstruction at decadal scales. For instance, Collins et al. (2019) show that the age uncertainty from MD07–3093 is around 51 years. However, this age uncertainty is much smaller than the temporal scale of multi-centuries that we focus on. Furthermore, a 0.5 °C error could provide stronger constraints on these long-term changes that highlight the differences between ASSIM-P2000-CON and ASSIM-P2000-ALL in which the marine records are not assimilated. As for the error of the sea ice persistence record in Adelie Land coast, it is calculated by computing the standard deviation of difference between the reconstructed sea ice persistence using the transfer equation established by Crosta et al. (2021) and the observed length of the yearly sea-ice free season off Adelie Land between 1979 and 2010 as reported by Campagne et al. (2016).

2.4. Experimental design

To investigate the impact of temporal resolution on the assimilation results, we conducted two data assimilation (DA) experiments covering the past two centuries. The experiments, named ASSIM-P200-1 yr and

ASSIM-P200-10 yr, utilized the same ice-core based δ18O and snow accumulation records as well as Southern Hemisphere tree ring width records (refer to Fig. S1 and Table 2) and followed the methodology of Dalaiden et al. (2021).

For the experiments covering the past two millennia, we assimilated both the continental proxy records and the marine records (i.e., Southern Ocean SST reconstructions) as explained in Section 2.1 (Fig. 1). To further distinguish the influence of continental and marine records on the reconstruction, we separately perform two DA experiments. ASSIM-P2000-CON assimilated only continental proxies, while ASSIM-P2000-ALL assimilated all available records. We also performed the ASSIM-P2000-DJF experiment to test the sensitivity of the DA-based reconstruction to the seasonality of SST reconstructions. In this experiment, we assumed the reconstructed SST to represent summer conditions by utilizing the mean over December, January, and February as prior modeling results. All experiments are summarized in Table 2.

We make quantitative comparisons by the computation of two statistical metrics. The first is the Pearson correlation coefficient (r value) and the related *P*-value. The second is the coefficient of efficiency (CE value):

$$CE = 1 - \sum_{i=1}^{n} \frac{(x_i - y_i)^2}{(x_i - \bar{x})^2}$$

where x_i is the "true" time series, $\bar{x}$ is the mean of the "true" time series over a reference period; and y_i is the reconstructed time series. This metric is used in Section 3.1. The upper limit of CE is 1, which indicates that the two time series have the same variations in both amplitude and timing, while negative CE values result from a bias between the two datasets, in either the mean or amplitude of the variability.

3. Results and discussion

3.1. Evaluation of the skill of the reconstructions over the past 200 years

We first assess the sensitivity of the results to the temporal resolution

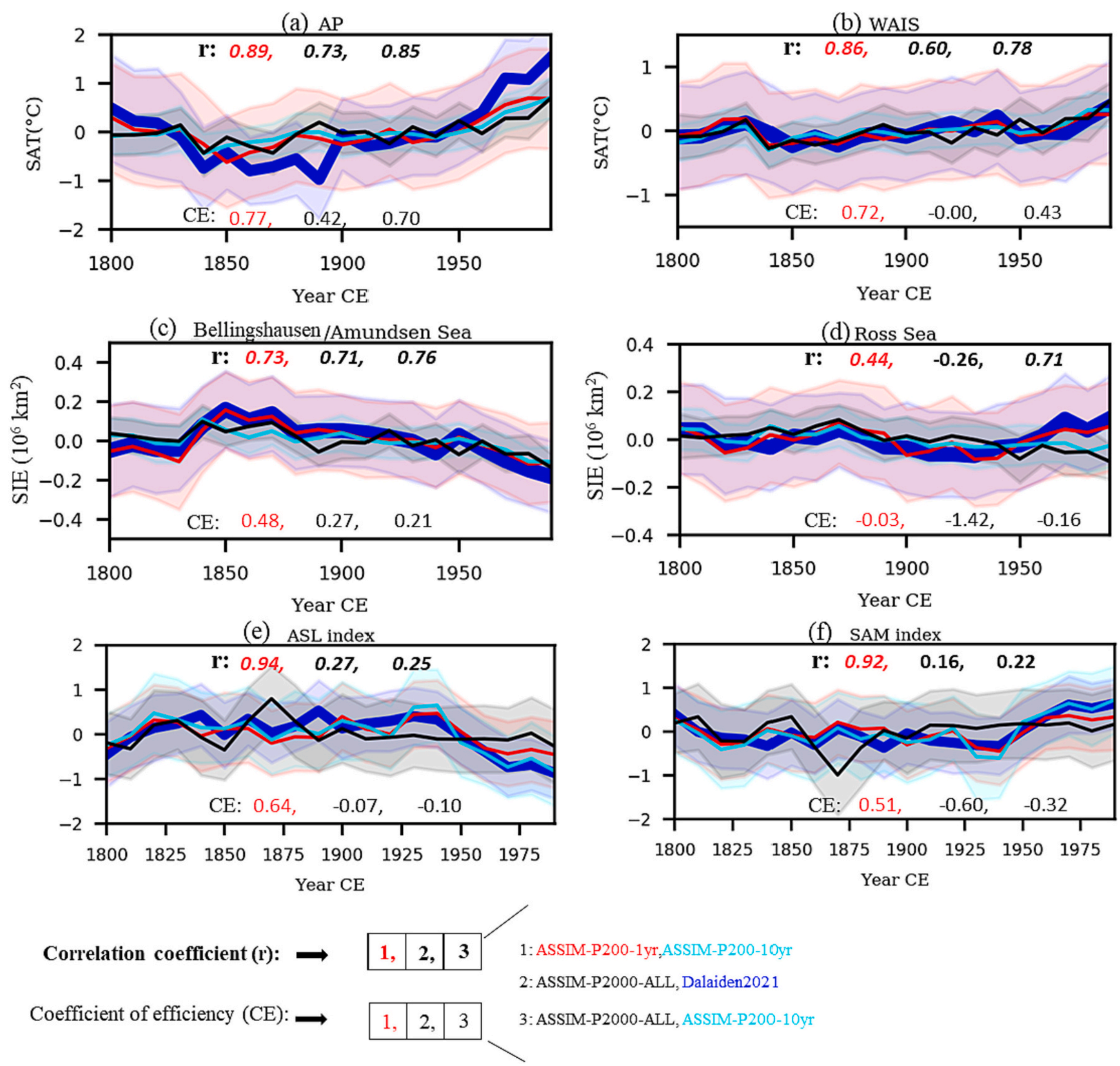

Fig. 2. Comparisons for the surface air temperature (SAT) over the Antarctic Peninsula (AP, a) and the West Antarctic Ice Sheet (WAIS, b), for the sea ice extent (SIE) integrated in the Bellingshausen/Amundsen sea sector (c) and the Ross Sea sector (d), and for the Amundsen Sea Low index (ASL, e) and the Southern Annual Mode index (SAM, f), over the past two centuries, between various reconstructions from this study, i.e., ASSIM-P200-1 yr (red), ASSIM-P200-10 yr (cyan), ASSIM-P2000-ALL (black), and from Dalaiden et al. (2021, blue). All quantities are expressed in anomalies (relative to the 1800–2000 CE period). Shaded areas represent ±1 standard deviation of the DA-based reconstructions. Correlation coefficients (r) between different reconstructions are shown in bold (the statistically significant ones at $p < 0.05$ are shown in italic font) above the time series in each panel, while the others below the time series represent the values of coefficient of efficiency (CE). (For interpretation of the references to colour in this figure legend, the reader is referred to the web version of this article.)

(annual and decadal) of the assimilated observations. ASSIM-P200-1 yr and ASSIM-P200-10 yr show consistent results with high and statistically significant correlation coefficients between them and positive CE values for SAT over the AP ($r = 0.89$ at $p < 0.05$, CE = 0.77) and WAIS ($r = 0.86$ at $p < 0.05$, CE = 0.72), and for the SAM (0.94 at $p < 0.05$, CE = 0.64) and ASL index (0.92 at p < 0.05, CE = 0.64) over the past two centuries (Fig. 2). The correlation coefficients between the local SAT and sea level pressure are also high and significant at many locations in the domain (Fig. 3a and b).

For the SIE, The Bellingshausen/Amundsen sector shows clear similarity between the experiments ($r = 0.73$ at $p < 0.05$, CE = 0.48), but larger differences are seen in the SIE (sea ice extent) integrated over the Ross Sea sector. Here, we observe a relatively small correlation coefficient ($r = 0.44$ at p < 0.05) and negative CE value (−0.03). The spatial distribution shows low correlations on the northern edge of the Ross Sea and near the coast of the western part of the Amundsen Sea (Fig. 3c), where the correlation coefficients between the two experiments are not significant.

The results appear insensitive to the temporal resolution of the records, except for sea ice concentration in some regions. This discrepancy may be due to the time scale-dependent covariance between variables. To clarify this concept, we calculate correlation coefficients, which can be seen as the covariance normalized by the product of the standard deviations, between SIE, SAT, and the ASL. To remove the influence of the global warming over the past century, we use detrended time series (denoted by r_d in Fig. 4) and calculate correlation coefficients over the Ross Sea sector (160°E-130°W, 50°S-70°S), where the discrepancy is most notable.

Significant negative correlation coefficients are found between the ASL and SIE in the Ross Sea sector ($r = -0.88$ at p < 0.05; $r_d = -0.92$ at p < 0.05) in ASSIM-P200-1 yr (Fig. 4). This highlights the strong control of the ASL on the SIE over the Ross Sea sector through atmospheric processes at interannual scale, as proposed in several previous studies (e.g., Hosking et al., 2013; Raphael et al., 2019; Dalaiden et al., 2021). For instance, a deeper ASL results in stronger cold southerly winds that transport sea ice off the Ross Sea, leading to a larger regional SIE. In contrast, ASSIM-P200-10 yr shows a non-significant correlation coefficient of 0.09. However, the correlation based on the detrended time series is still negative (rd = −0.44 at p < 0.05), although much smaller than that of ASSIM-P200-1 yr.

The next step is to investigate changes in oceanic temperatures at 100 m and 500 m water depths, recognizing that the ocean's large thermal inertia and delayed response to disturbances, relative to the atmosphere, may account for this time dependence. We obtained these two variables from our reconstructions by utilizing the link between the variables we directly assimilate (i.e., SMB, δ^{18}O, SST, and sea ice persistence) and the oceanic temperature at 100 m and 500 m water depths, deduced from the model physics (i.e., iCESM1). In ASSIM-P200-10 yr, the SIE in the Ross Sea sector is negatively correlated to oceanic temperature at both 100 m ($r = -0.74$ at $p < 0.05$; $r_d = -0.37$ at p < 0.05) and 500 m ($r = -0.66$ at p < 0.05; $r_d = -0.26$ at $p > 0.05$). However, in ASSIM-P200-1 yr, a significant negative correlation only occurs between the SIE and oceanic temperature at 100 m ($r = -0.51$ at $p < 0.05$; $r_d = -0.70$ at p < 0.05), while an insignificant positive correlation coefficient is obtained between the SIE and oceanic temperature at 500 m ($r = 0.29$ at p > 0.05; $r_d = 0.44$ at p < 0.05). In other words, an

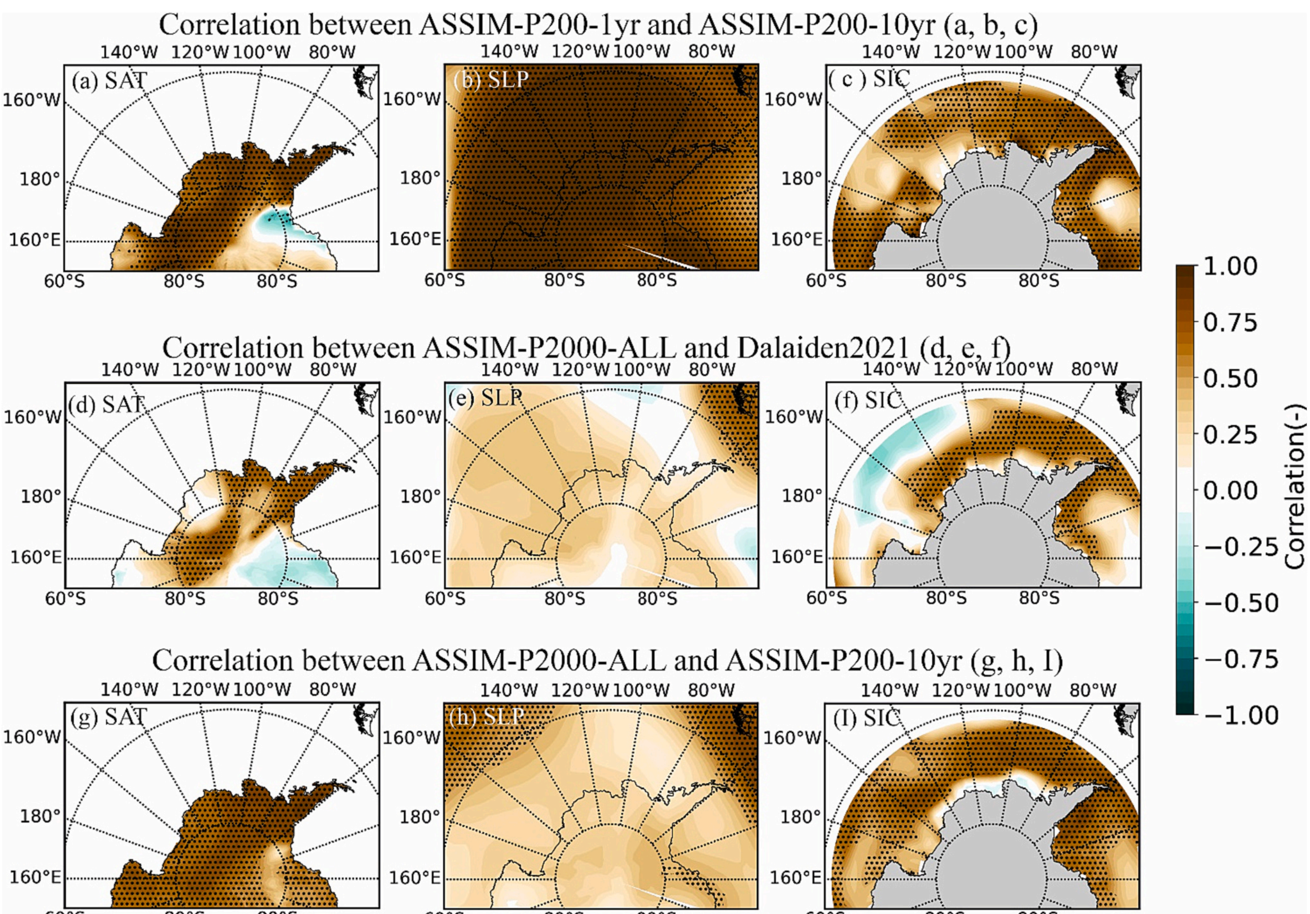

Fig. 3. Spatial patterns of the correlation coefficients for the surface air temperature (SAT), sea level pressure (SLP), and sea ice concentration (SIC) between ASSIM-P200-1 yr and ASSIM-P200-10 yr (a, b, c), between ASSIM-P2000-ALL and the reconstruction from Dalaiden et al. (2021) (d, e, f), and between ASSIM-P2000-ALL and ASSIM-P200-10 yr (g, h, i). The stippled area indicates the correlation coefficients at a 95% confidence level ($p < 0.05$).

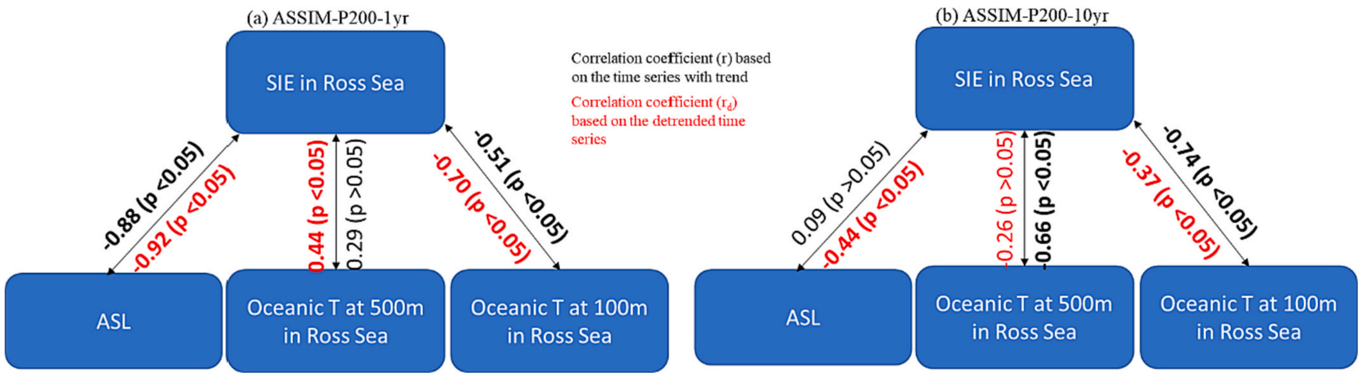

Fig. 4. The correlation coefficients between sea-ice extent (SIE) in the Ross Sea sector and ASL, the subsurface oceanic temperature at 100 m and 500 m (their time series are shown in Fig. S2), respectively, presented in the reconstructions of ASSIM-P200-1 yr (a) and ASSIM-P200-10 yr (b).

increase in SIE in the Ross Sea is associated with a cooling of the water column up to 500 m in ASSIM-P200-10 yr, while the cooling is restricted to the upper layers in ASSIMP200-1 yr.

The results suggest that on the interannual timescale, only the upper ocean interacts with the surface while the deeper ocean plays an important role on the decadal time scale. Ferreira et al. (2015) proposed that the Southern Ocean's response to winds could be timescale dependent. An atmospheric pattern similar to a positive SAM triggers short-term cooling at the interannual scale by horizontal Ekman drift, followed by slower warming around Antarctica induced by Ekman upwelling of warmer water. Such a mechanism may induce different covariances between the variables as a function of the timescale. Our findings support the hypothesis that the upwelling of deeper waters plays a strong role on longer timescales (e.g., Ferreira et al., 2015). However, this correlation analysis does not establish a causality link, and our purpose is not to delve deeper into the physical mechanism. Our results highlight the importance of co-variability between state variables in the DA process, and the need to evaluate the validity of the model-derived covariance for each application, especially when reconstructing sea ice or other oceanic variables (Tardif et al., 2014, 2015; Steiger and Hakim, 2016). Since there are no long-term sea ice observations over the past two centuries (e.g., Vorrath et al., 2020), it is impossible to determine which reconstruction (ASSIM-P200-1 yr or ASSIM-P200-10 yr) is more accurate. Nonetheless, to better integrate the role of the ocean on the system's low-frequency variability, using a 10-year assimilation window for the assimilation seems reasonable.

Ideally, our reconstruction covering the past 2000 years should be compared to observations, but due to the decadal resolution of ASSIM-P2000-ALL and the short length of instrumental data covering the past 2–3 decades, there are only 2–3 degrees of freedom remaining if observations are averaged using a 10-year window. Alternatively, we compare ASSIM-P2000-ALL to the reconstruction of Dalaiden et al. (2021), which has been shown to provide skillful reconstructions of atmospheric circulation, sea ice concentration, and SAT over the past 200 years in the West Antarctic sector. Dalaiden et al. (2021) assimilated the same records as in ASSIM-P200-1 yr, using the same methodology but with additional records from East Antarctica. Dalaiden et al. (2021) and ASSIM-P200-1 yr are thus very similar in West Antarctica (see the comparison between Dalaiden et al. (2021) and ASSIM-P200-1 yr in Fig. S3). In addition, we compare ASSIM-P2000-ALL and ASSIM-P200-10 yr to evaluate the contribution of the number of proxies. It is important to note that no marine record is assimilated in ASSIM-P2000-ALL over the period 1800–2000 CE and thus there is no difference between ASSIM-P2000-ALL and ASSIM-P2000-CON for this period.

The spatial SAT reconstructions (Fig. 3d) reveal that ASSIM-P2000-ALL is significantly correlated with Dalaiden et al. (2021) over the AP region ($r = 0.73$ at $p < 0.05$; CE = 0.42 for the sub-region mean, Fig. 2a). Over the WAIS, however, some small zones with non-significant correlations are observed in the western and central part of the region. This could be due to the poor performance of ASSIM-P2000-ALL in the reconstruction of the atmospheric circulation (Fig. 3e), in particular for the SAM (Fig. 2f) and ASL index (Fig. 2e). Consequently, the CE value is close to zero for the WAIS mean, but a significant correlation coefficient (0.60 at $p < 0.05$) indicates that ASSIM-P2000-ALL captures the general trend over the past two centuries, as reconstructed in Dalaiden et al. (2021). Comparing ASSIM-P2000-ALL to ASSIM-P200-10 yr, remarkable consistency is seen in West Antarctica (Fig. 3g). The correlation coefficients between ASSIM-P2000-ALL and ASSIM-P200-10y are 0.85 ($p < 0.05$) over the AP, and 0.78 ($p < 0.05$) over the WAIS. The positive CE values indicate that the magnitude of the decadal variability is similar between both reconstructions. This suggests that the differences between ASSIM-P2000-ALL and Dalaiden et al. (2021) are due to the temporal resolution rather than the number of records.

ASSIM-P2000-ALL shows a strong correlation with Dalaiden et al. (2021) for sea ice concentration in the Bellingshausen/Amundsen Sea, but in the Ross Sea, there are large areas with negative correlation coefficients. In contrast, ASSIM-P200-10 yr and ASSIM-P2000-ALL display good agreement over almost the entire high-latitude Pacific sector of the Southern Ocean (Fig. 3i), indicating that the differences between ASSIM-P2000-ALL and Dalaiden et al. (2021) are due to the temporal resolution. Concerning the reconstruction of the SIE integrated over the Bellingshausen/Amundsen Sea, ASSIM-P2000-ALL seems skillful when compared to Dalaiden et al. (2021) ($r = 0.71$ at $p < 0.05$, CE = 0.27) and ASSIM-P200-10 yr ($r = 0.76$ at $p < 0.05$, CE = 0.21) (Fig. 2c). However, for the reconstruction of SIE over the Ross Sea, ASSIM-P2000-ALL shows negative CE values when compared to Dalaiden et al. (2021) (−1.42) and ASSIM-P200-10 yr (−0.16) (Fig. 2d). Nonetheless, the high correlation coefficient between ASSIM-P2000-ALL and ASSIM-P200-10 yr (0.71 at $p < 0.05$) indicates that assimilating only a few records in ASSIM-P2000-ALL is still able to capture the general trend of SIE over the Ross Sea for the past two centuries, even though the magnitude of the changes may be less trustworthy than in ASSIM-P200-10 yr.

For the sea level pressure over West Antarctica and its surrounding seas in the Southern Ocean, ASSIM-P2000-ALL correlates positively, but not significantly, with both Dalaiden et al. (2021) and ASSIM-P200-10 yr (Fig. 3e and h). This suggests that the number of records included in ASSIM-P2000-ALL might be too low and that the use of this reconstruction variable should be treated with caution.

3.2. *Surface temperature and sea ice changes in West Antarctica and its surrounding seas over the past two millennia*

The evolution of SAT and SIE in the West Antarctic sector over the past two millennia from ASSIM-P2000-ALL and ASSIM-P2000-CON is displayed in Fig. 5. and they appear quite similar, particularly during the first millennium. There are relatively small centennial fluctuations in the

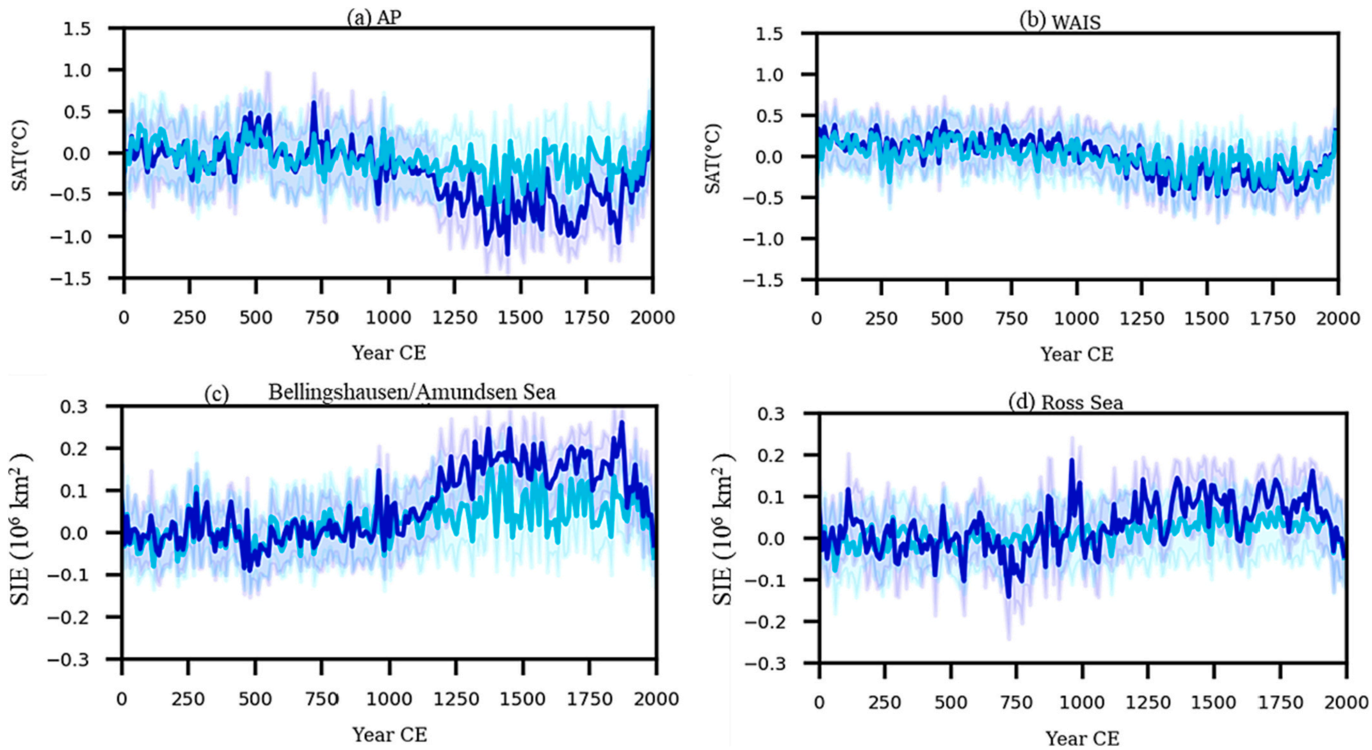

Fig. 5. The surface air temperature (SAT) anomalies (in °C relative to 1–2000 CE) over the Antarctic Peninsula (AP, a) and the West Antarctic Ice Sheet (WAIS, b), and the sea ice extent (SIE) anomalies (in 10^6 km^2 relative to 1–2000 CE) integrated over the Bellingshausen/Amundsen/ Sea sector (c) and the Ross Sea sector (d) derived from the ASSIM-P2000-ALL (blue) and ASSIM-P2000-CON (cyan) reconstructions. The shaded areas represent ±1 standard deviation of the DA-based reconstructions. (For interpretation of the references to colour in this figure legend, the reader is referred to the web version of this article.)

SAT and SIE over the years 1–400 CE. Subsequently, the warmest period over the first millennium is observed between 450 and 550 CE, followed by a significant cooling to 1000 CE over the WAIS and AP. This result is consistent with previous reconstructions by Lyu et al. (2021) that focus on multi-centennial trends in the SAT over Antarctica during the first millennium, indicating that the assimilation of the marine records in ASSIM-P2000-ALL brings additional constraints for the first millennium that are compatible with those in ASSIM-P2000-CON. This confirms the robust SAT reconstruction of Lyu et al. (2021) for the first millennium over West Antarctica.

In contrast to the evolution over the first millennium, we observe large centennial or multi-centennial fluctuations in the SIE and SAT for the second millennium (i.e., 850–1850 CE), with larger amplitude changes in ASSIM-P2000-ALL compared to ASSIM-P2000-CON. Accordingly, we focus on this period in the remaining part of the study. We observe significant differences in mean SAT and SIE between the 1400–1800 CE and 900–1300 CE periods. These two multi-centennial intervals are brought in phase with the LIA and MCA in the North Hemisphere (Mann et al., 2009), respectively, although different time intervals have historically been defined in the literature (Neukom et al., 2019a). Furthermore, the SAT and SIE reconstructions in ASSIM-P2000-ALL have good agreement with those in the sensitivity experiment (ASSIM-P2000-DJF, with correlations larger than 0.7 at $p < 0.05$), when the assimilated SST reconstructions are considered to represent summer temperatures, rather than annual ones (Fig. S4). This implies that although SST reconstructions are assumed to provide information only for summer, DA remains able to reconstruct the changes in the annual mean, albeit with a smaller magnitude.

Both ASSIM-P2000-ALL and ASSIM-P2000-CON show a long-term cooling trend from the MCA to LIA periods in the SAT over the AP. However, the cooling is more pronounced in ASSIM-P2000-ALL (0.42 °C) than in ASSIM-P2000-CON (0.08 °C). Over the WAIS, the difference between the two reconstructions is smaller, but the cooling is still more significant in ASSIM-P2000-ALL (0.27 °C) than in ASSIM-P2000-CON (0.13 °C). Consistent with the regional cooling in the West Antarctic sector, the SIE displays an expansion of 0.12 10^6 km^2 in the Bellingshausen/Amundsen Sea during the LIA relative to the MCA in ASSIM-P2000-ALL and of 0.03 10^6 km^2 in ASSIM-P2000-CON. In the Ross Sea, both reconstructions show a smaller difference in the evolution of SIE from the MCA to LIA periods, with ASSIM-P2000-ALL and ASSIM-P2000-CON indicating an SIE increase of 0.05 10^6 km^2 and 0.02 10^6 km^2, respectively.

To understand the differences between the reconstructions, it is useful to compare them to the four SST reconstructions located on the southern Chilean coast that are assimilated in ASSIM-P2000-CON but not in ASSIM-P2000-ALL. As expected, the SST reconstructions in ASSIM-P2000-ALL display high correlation coefficients with the original ones, indicating the effectiveness of the DA process in the reconstruction (see Fig. 6). Interestingly, despite the fact that ASSIM-P2000-CON does not directly assimilate the SST reconstructions, the correlation coefficients between the DA-based reconstruction and the SST reconstructions remain significant and close to 0.5. This suggests that the information provided by the continental proxy records assimilated in ASSIM-P2000-CON is consistent with the information provided by the SST reconstructions, particularly with regard to the long-term cooling trend over the last millennium.

However, a visual comparison of the time series in Fig. 6 clearly shows that our SST reconstructions underestimate the centennial variability compared to the original SST records, regardless of whether those SST reconstructions are assimilated. This potential underestimation of the variability is a common issue for DA reconstructions (e.g., Tardif et al., 2019). In this case, it is likely due to a more general problem of climate models that underestimate the variance at the local scale compared to marine proxies (e.g., McGregor et al., 2015). On the other hand, the SST reconstructions could also contain non-climatic information, and could suffer from methodological uncertainties (e.g.,

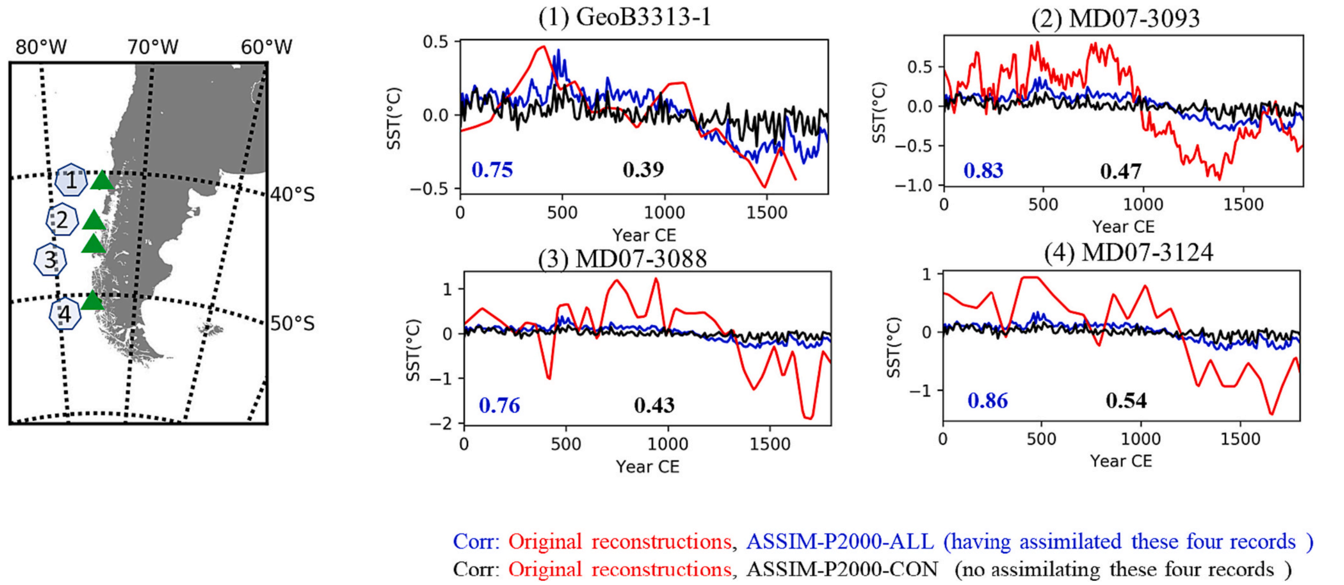

Fig. 6. Comparison between the original SST reconstructions (anomalies over 1–1800 CE) (red) derived from the marine records located at the southern Chilean coast (as shown in the left map) and the reconstructions from ASSIM-P2000-ALL (blue) and ASSIM-P2000-CON (black). These four records are assimilated in ASSIM-P2000-ALL, but not in ASSIM-P2000-CON. The numbers within each subplot correspond to the correlation coefficients between the original SST reconstructions and ASSIM-P2000-ALL (blue) and ASSIM-P2000-CON (black). (For interpretation of the references to colour in this figure legend, the reader is referred to the web version of this article.)

calibration, seasonality, and other processes affecting local and seasonal production of alkenones). As a consequence, the model ensemble (i.e., the prior) does not include states that present enough large anomalies compared to the data. The filter selects the particles that have a strong signal at the location of the proxies but this is still significantly different compared to that provided by the SST reconstructions. Nevertheless, one consequence of assimilating the marine proxy records is to amplify the variability locally in ASSIM-P2000-ALL at the location where marine proxies are available. Consequently, it amplifies the variability at larger scales, which explains the larger changes in temperature over WAIS and the AP and the larger increase in sea ice concentration between the MCA and the LIA in the Bellingshausen/Amundsen Sea in this experiment.

Comparing ASSIM-P2000-CON and ASSIM-P2000-ALL to independent reconstructions based on marine sediments is a useful way to evaluate their relative performance (see Fig. 7). The high abundance of sea ice sensitive diatom taxa normally reflects sea ice expansion or persistent sea ice existence during that period (Crosta et al., 2021). Most of the sea-ice related diatom records around the AP coast (5/7, including GEBRA-1, GEBRA-2, JPC127, JPC38, and JPC10) show a common signal with a clear increase in sea ice over the past millennium. The sea ice concentration at the locations of these five diatom records, as reconstructed in ASSIM-P2000-ALL, appears to follow the increasing trend

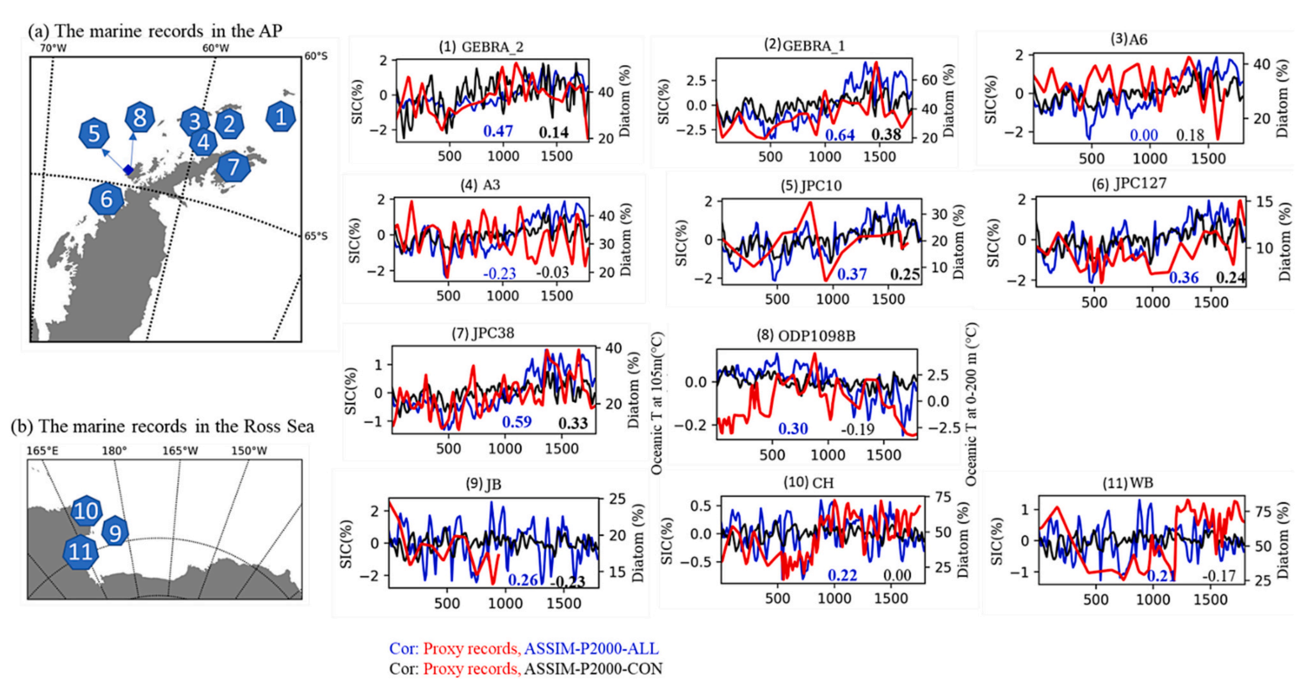

Fig. 7. Same as Fig. 6, but for the marine records in the Antarctica Peninsula (AP, a) and the Ross Sea (b) used for the validation.

better than the reconstructions in ASSIM-P2000-CON. This is evidenced by the higher correlation coefficients between the diatom records and ASSIM-P2000-ALL (on average 0.52 at $p < 0.05$) compared to ASSIM-P2000-CON (on average 0.27 at $p < 0.05$).

In addition, we have conducted a comparison of our reconstruction with a TEX86-based (sub)surface sea temperature record, as depicted in Fig. 7 (8). It is important to note that the interpretation of this particular record remains subject to ongoing debate. In their study, Etourneau et al. (2013) analyzed a new TEX86-SST record obtained from core JPC-10, located at 64° 53'S, 64°12'W, which is in proximity to ODP Hole 1098. They observed discrepancies in temperature estimates, both in terms of amplitude and variations, when compared to the findings published by Shevenell et al. (2011). Furthermore, Etourneau et al. (2013) did not calibrate the TEX86 index against sea surface temperature directly, but rather against the mean temperature integrated over the 0–200 m water depth. Therefore, in our analysis, we compare our reconstruction of oceanic temperature at a depth of 105 m with this particular TEX86-based reconstruction. Fig. 7 (8) reveals that while there are notable differences in the multi-centennial trend during the first millennia between our reconstruction and Shevenell et al. (2011), there is a consistent indication of significant cooling over the past millennium, particularly when comparing ASSIM-P2000-ALL with the TEX86-based reconstruction. This finding supports the presence of a cooling trend and adds further credibility to our own reconstruction. We have identified inconsistencies between our reconstructions and two records located in the Bransfield Basin, which we refer to as A3 and A6 in the following text and Fig. 7. In contrast to our reconstructions of the region, A3 and A6 records display no significant trend for the past millennium, resulting in correlation coefficients close to zero. Furthermore, A3 and A6 are inconsistent with other diatom records, particularly with GEBRA-1, which is also located in the Bransfield Channel to the east of A3 and A6. These discrepancies highlight the complexity of local dynamics in this region and the interpretation of diatom records. The sea ice information preserved in the sediments of A3 and A6 may have been affected by the seasonality of sea ice conditions and/or the upwelling of deep warm water (Bárcena et al., 1998) in the western Bransfield Strait, which could have masked the large-scale climatic signal observed in other records.

We compare our reconstructions to three marine diatom records in the western Ross Sea. Over the past two millennia, the sea ice

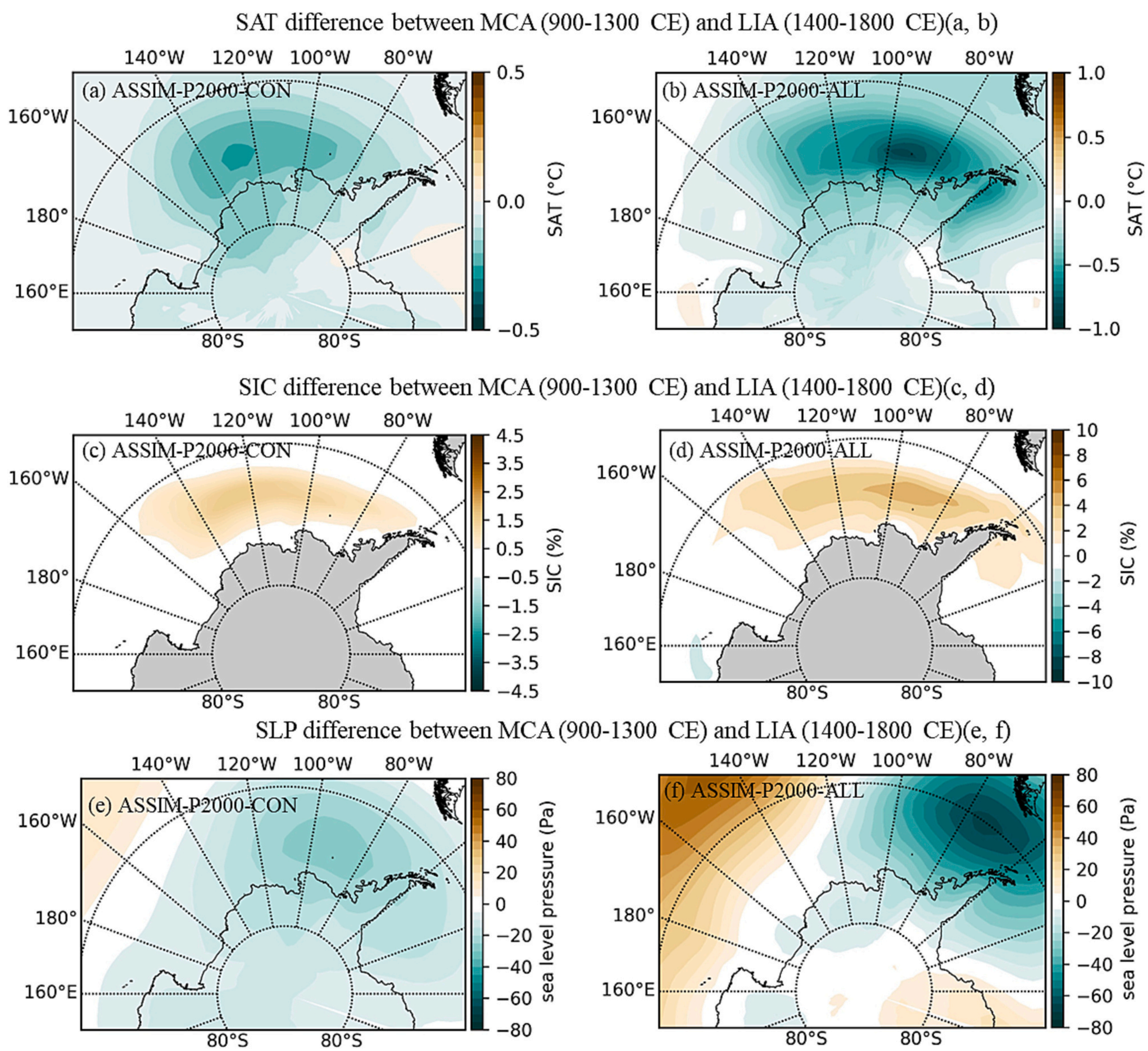

Fig. 8. Spatial patterns of the LIA (1400–1800 CE)-MCA (900–1300 CE) difference in the SAT (a, b), SIC (c, d), and SLP (e, f) derived from ASSIM-P2000-CON and ASSIM-P2000-ALL. Note, the colour bar is independent for each subplot to make the pattern visually readable.

concentration derived from ASSIM-P2000-ALL at three proxy sites positively correlates with the original records, although the values are relatively small (between 0.20 and 0.26). The correlation coefficients between ASSIM-P2000-CON and those proxy records are lower and are even negative for two of them (0.0 in the third one). The original study describing these three diatom records identified the important role of katabatic winds and latent-heat polynyas on the coastal sea ice in this region (Mezgec et al., 2017). However, the general circulation model used in the DA process is unable to simulate and capture those small-scale coupled ocean-atmosphere processes. This may explain the relatively poor agreement between our reconstructions and the proxy records in the Ross Sea region.

3.3. Is there a widespread cooling over WA and adjacent seas for the past millennium?

Here we investigate the spatial distribution of several key variables (i.e., sea ice concentration, sea level pressure, and SAT) to examine whether there was a widespread cooling over West Antarctica and adjacent seas for the past millennium in our two reconstructions and the potential associated mechanisms (Fig. 8). Compared to the localized cooling zone in the western WAIS shown in the ASSIM-P2000-CON reconstruction (Fig. 8a), the ASSIM-P2000-ALL reconstruction shows more extensive and intense cooling over West Antarctica. The sea ice concentration pattern is consistent with that of SAT, with a more substantial sea ice concentration increase over the Pacific sector of the high latitudes of the Southern Ocean in ASSIM-P2000-ALL than in ASSIM-P2000-CON.

The changes in the reconstructed atmospheric circulation exhibit clear differences between the two experiments, but both display a decrease in sea level pressure over the Bellingshausen Sea between the MCA and the LIA, with an eastward shift and deepening of the low-pressure system in the ASSIM-P2000-ALL compared to ASSIM-P2000-CON. Despite significant disparities in both the magnitude and patterns of sea level pressure changes between the reconstructions and the limited skill exhibited by our reconstruction for this variable over the past 200 years (as illustrated in Fig. 3), it remains valuable to examine the influence of these sea level pressure variations on regional temperatures. Specifically, as the ASL is known to be a major contributor to the variability in the region, we have performed a congruence analysis to identify the contribution of the ASL to the changes in the SAT during the LIA-MCA transition. This methodology is the same as the one in previous studies, e.g., Jones et al. (2019). We first derive the ASL index from our reconstructions and then perform a linear regression between the ASL index and the SAT for each grid cell after removing linear trends over the 900–1800 CE period. We finally multiply the SAT sensitivities derived from the regression by the trends in the ASL index over 900–1800 CE to estimate the ASL-congruent SAT changes. In both reconstructions, the SAT congruent trend shows a small cooling over the WAIS but with signals of different signs over the AP (Fig. 9). Nevertheless, the values are relatively low indicating that the ASL plays a relatively small role in the cooling trend in our reconstructions.

The general cooling in West Antarctica and adjacent seas obtained in our reconstructions between the LIA and the MCA is consistent with the iCESM1 ensemble mean (Fig. 10) as well as with other simulations performed with climate models (e.g., LOVECLIM in Goosse et al., 2012, models in PMIP3/CMIP5 as shown in Klein et al., 2019). The magnitude of the changes in iCESM1 is actually very close to that in ASSIM-P2000-ALL, the reconstruction that appears the most accurate for the long-term trend over the past millennium as shown in Section 3.2, and larger than in ASSIM-P2000-CON, in particular over the AP. This suggests that the widespread cooling over West Antarctica and the Pacific sector of the Southern Ocean in ASSIM-P2000-ALL is driven by external forcings and corresponds to a standard response to the decrease in the global radiative forcing between the two periods. Goosse et al. (2012) and Phipps et al. (2013) suggest that volcanic forcing is the main contributor to this cooling trend over Antarctica and the Southern Hemisphere for the last millennium. Here we confirm this conclusion by examining the simulations driven by all forcings and by only the volcanic forcing performed with the CESM1 (Fig. S5, Otto-Bliesner et al., 2016). Over 900–1800 CE, the ensemble mean of CESM1 driven by all the forcings shows a significant cooling trend with −0.04 °C/100 yr in the AP and − 0.05 °C/100 yr in the WAIS. >50% of this cooling trend is obtained in the simulations conducted using only the volcanic forcing, with −0.02 °C/100 yr in the AP and − 0.03 °C/100 yr in the WAIS, highlighting the dominant influence of this forcing on the widespread MCA-LIA cooling over West Antarctica and the surrounding seas.

Our ASSIM-P2000-ALL and ASSIM-P2000-CON agree also relatively well with the one of Stenni et al. (2017) in WAIS, which also displays a significant cooling there (−0.06 °C/100 yr at $p < 0.05$). However, the slight warming of 0.01 °C/100 yr (at $p > 0.05$) in the AP present in the Stenni et al. (2017) reconstruction contrasts with the cooling present in both our reconstructions. Assimilating the same continental proxy records as in ASSIM-P2000-CON but with annual resolution (Fig. S6) reproduces the weak warming shown in Stenni et al. (2017) because of a larger contribution of the changes in the ASL (ASL-congruent trend 0.02 °C/100 yr). However, this additional experiment shows less agreement with the independent sea-ice proxy records than ASSIM-P2000-CON and ASSIM-P2000-ALL, indicating that it is likely not able to reproduce the centennial variability in the AP region.

Since our reconstructions and Stenni et al. (2017) include only one high-resolution $\delta^{18}O$ record covering the past two millennia in the AP from the ice core collected on the James Ross Island (JRI), it is interesting to investigate how this record constrains our reconstructions. The correlation between the original $\delta^{18}O$ record and the reconstructed one from ASSIM-P2000-CON (0.86, $p < 0.05$) is much higher than the

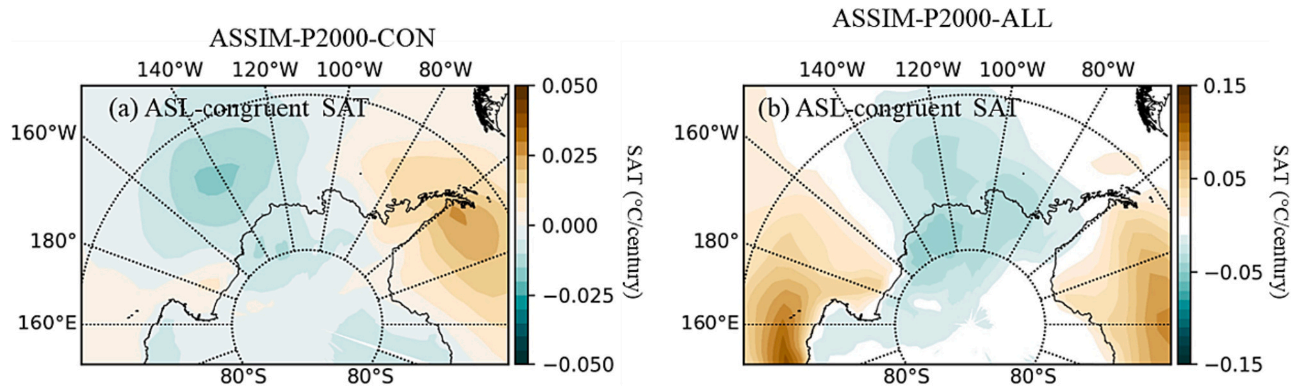

Fig. 9. Spatial patterns for the ASL-congruent trend in the SAT derived from ASSIM-P2000-CON (a) and ASSIM-P2000-ALL (b). Note, the colour bar is independent for each subplot to make the pattern visually readable.

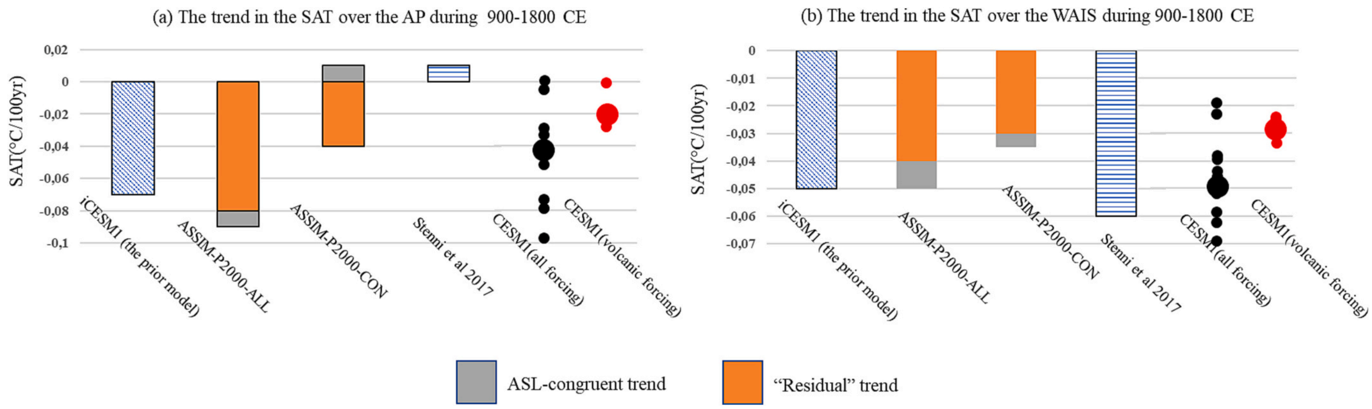

Fig. 10. The area-weighted mean of ASL-congruent and "residual" trend in the SAT from ASSIM-P2000-ALL, ASSIM-P2000-CON, and the trend from iCESM1 and CESM1 (including all forced simulations and volcanic-forced simulations) over the AP (a) and WAIS (b).

correlation with ASSIM-P2000-ALL (0.46, $p < 0.05$) over the last two millennia. Furthermore, ASSIM-P2000-ALL displays a negative trend of −0.24 per mill/century ($p < 0.05$) in the $\delta^{18}O$ at JRI over 900–1800 CE, while ASSIM-P2000-CON has no trend (0.00 per mil/century, $p > 0.05$) and the original $\delta^{18}O$ has a positive one (0.3 per mil/century, $p < 0.05$, Fig. S6), consistent with the reconstruction of Stenni et al. (2017) which is based on this record. There are also large differences between both reconstructions in the trend of the snow accumulation at JRI, with −44.8 Gt year^{-1} per century ($p < 0.05$) in ASSIM-P2000-ALL and 14.7 Gt year^{-1} per century ($p < 0.05$) in ASSIM-P2000-CON (Fig. S6). This confirms that the reconstruction in ASSIM-P2000-ALL is much less controlled by the JRI record because of the additional information provided by the marine data, while ASSIM-P2000-ALL and especially the Stenni et al. (2017) reconstruction critically depends on this single record.

As there have been some debates about the temperature trends over the past millennium, the synchronicity between regions and even the existence of a transition between warmer and colder periods such as the MCA and the LIA (Neukom et al., 2019a; PAGES 2k-PMIP3 group, 2015), we examine the relationship between our reconstructions for the 10-year averaged SAT over West Antarctica and the global SAT reconstructions of Neukom et al. (2019b) over the past millennium (850–1850 CE) (Figs. 11 and S7). The results show that the global SAT correlates much better with the reconstructions in ASSIM-P2000-ALL (0.65 at zero lag) than with ASSIM-P2000-CON (0.35 at zero lag). It is sometimes argued that the Antarctic response to forcings may lag significantly behind the global one (e.g., Abram et al., 2016), but this does not seem to be the case for West Antarctica as the maximum correlation between the ASSIM-P2000-ALL and global SAT occurs for a lag of 20 years only (global temperature leading). By contrast, when we compute the same metrics but with the detrended time series, we find a poor relationship between our reconstructions and the global SAT. In addition, we also make a comparison of the recent warming between the reconstructions. The global reconstruction shows a warming trend starting around 1800 based on the 100-year averaged time series, which is very close to the one in ASSIM-P2000-ALL with a warming starting around the same time (Fig. 11). This suggests that the synchrony between the global-averaged signal in Neukom et al. (2019b) and the one over West Antarctica in ASSIM-P2000-ALL exists not only for the cooling over the past millennium related to the dominant role of the volcanic forcing, but also for the recent warming at centennial-scale. This confirms that the centennial-scale temperature evolution over West Antarctica is coherent with global changes over the full past millennium.

However, the MCA–LIA temperature difference given by the global reconstruction is −0.16 °C, much smaller than the one over West Antarctica in ASSIM-P2000-ALL which reaches −0.31 °C. Additionally,

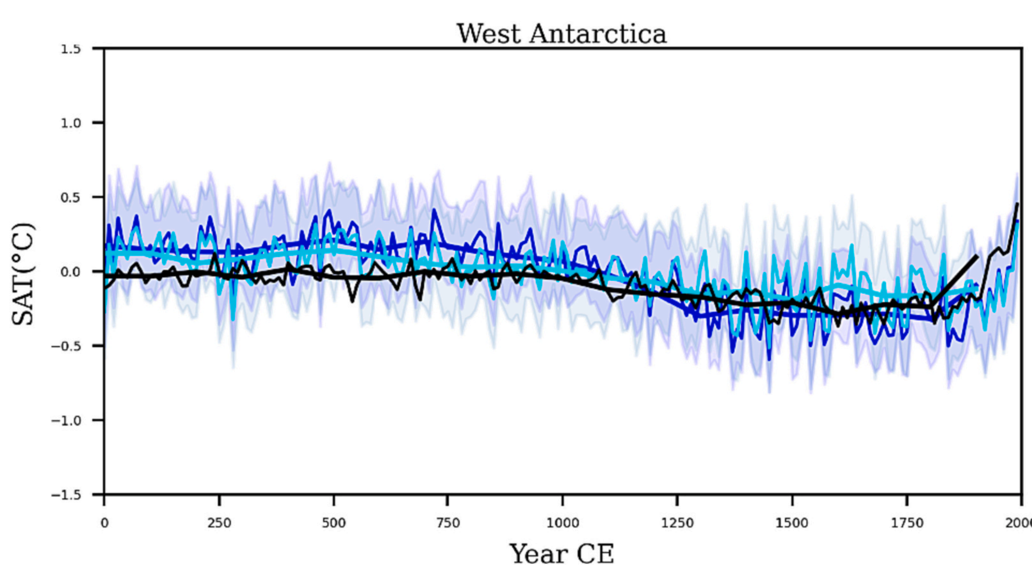

Fig. 11. The time series for the global-scale temperature from Neukom et al. (2019b) (black) and the reconstructed SAT over West Antarctica in ASSIM-P2000-ALL (blue) and ASSIM-P2000-CON (cyan). The thin line denotes the 10-year averaged time series, while the thick line represents the 100-year averaged time series. (For interpretation of the references to colour in this figure legend, the reader is referred to the web version of this article.)

the warming trend over the 20th century over West Antarctica in ASSIM-P2000-ALL is 0.60 °C/century, which is slightly larger than the global warming trend of 0.52 °C/century. We note again that there is no assimilation of the marine records during 1800–2000 CE, and hereby the magnitude of this trend over the 20th century over West Antarctica is likely underestimated based on the validation against Dalaiden et al. (2020) mentioned in Section 3.1. These differences between the amplitude of the variations between global-mean and WAIS could be interpreted as a moderate polar amplification of temperature changes, applied here for the Southern Hemisphere (Pithan and Mauritsen, 2014; Manabe and Wetherald, 1975; Goosse et al., 2018). For instance, the expanded sea ice over the Bellingshausen/Amundsen Sea during the LIA would enhance surface albedo and thus amplify the initial cooling by surface albedo feedback.

The analyses of the trend over the past millennium have highlighted the role of external forcing. Previous studies have proposed that unforced internal climate variability is also responsible for a large fraction of the changes (Goosse et al., 2012; Lyu et al., 2021), inducing complex patterns of cooling and warming for different periods. This explains the lack of coherence between global and West Antarctic temperatures for the detrended series over the past millennium. Additionally, as the external forcing, i.e., volcanism, is weaker during the first millennium, internal variability is likely dominant for this period. This is why no clear synchronous changes between West Antarctic temperature and global temperatures over the first millennium are found in our reconstructions.

4. Conclusion

In this paper, we investigate the climate variability over the past millennium in West Antarctica and surrounding seas by reconstructing several key climate variables (SAT, sea ice extent, and atmospheric circulation) using an offline DA method constrained by both continental and marine proxies. This approach enables us to generate internally consistent climate fields on the basis of the covariance between different variables.

Considering the dominant role of covariance relationships between variables in the DA process and their timescale dependence (Kunz and Laepple, 2021; Franzke et al., 2020), we compared two DA experiments that assimilate the same proxy records but with annual and decadal temporal resolutions (ASSIM-P200-1 yr and ASSIM-P200-10 yr). We confirm the existence of changes in covariance across timescales in our region of interest and show their impact on the reconstruction of some variables. For instance, previous studies (e.g., Hosking et al., 2013; Raphael et al., 2019) and ASSIM-P200-1 yr have shown a high correlation between the sea ice evolution in the Ross Sea and the Amundsen Sea Low at inter-annual scales over the past two centuries. However, our ASSIM-P200-10 yr experiment indicates that both variables have a more complex relationship at the decadal scale, especially when considering the trend over the past two centuries, and that sub-surface oceanic temperature seems to have a larger contribution to the sea ice variations in the Ross Sea region on those longer timescales. In this framework, the assimilation of continental and marine records at a uniform temporal resolution of 10 years provides a good compromise to combine the available low- and high-frequency records.

Our reconstructions covering the past two millennia (ASSIM-P2000-ALL and ASSIM-P2000-CON) reproduce the main characteristics of reconstructions performed over the past two centuries using a denser network of shorter time series proxy data (Dalaiden et al., 2021 and ASSIM-P200-10 yr) over their common period. However, some inconsistencies remain in atmospheric circulation and sea ice concentration in some parts of the Ross Sea. Nevertheless, the good agreement in terms of temporal and spatial variability of SAT and sea ice between ASSIM-P2000-ALL and ASSIM-P200-10 yr suggests that assimilating only a few records in those long reconstructions still provides valuable information for decadal-scale and longer climate variability over West Antarctica. Additionally, the comparison with independent sea ice-related marine records confirms the skillful reconstruction in terms of long-term variations, particularly when both continental and marine records are assimilated in ASSIM-P2000-ALL.

Our reconstruction, ASSIM-P2000-ALL, suggests that a widespread cooling trend occurred over West Antarctica and the surrounding seas from 900 to 1800 CE. This trend could be interpreted as the equivalent of the so-called transition between the MCA and the LIA in the region. Although the cooling trend over the WAIS is also present in many other reconstructions, the Stenni et al. (2017) reconstruction based on the JRI record does not display a cooling trend over the AP. It seems that including additional records in our reconstruction and taking advantage of the spatial covariance using a data assimilation framework gives less weight to the single JRI record. This cooling trend over the AP, present in ASSIM-P2000-ALL, is also consistent with several independent records (Lüning et al., 2019; Simms et al., 2021). Therefore, ASSIM-P2000-ALL likely provides a more accurate estimate of the large-scale changes in SAT in the AP region, but additional long records for the region would be extremely useful to confirm this hypothesis (e.g., Rowell et al., 2022).

This widespread cooling trend over the pre-industrial past millennium is also consistent with the climate modeling results which suggest that the cooling could be explained by a simple thermodynamic response to the radiative forcing evolution over the period. The contribution to long-term cooling from the SAM and ASL is relatively low. Analyzing ensembles of simulations driven by all the natural and anthropogenic forcings as well as an ensemble driven by only the volcanic forcing indicates a significant contribution of the latter to the cooling trend. Furthermore, the temperature changes over West Antarctica during the past two millennia are well correlated with the global mean surface temperature that has been shown to be strongly influenced by volcanic forcing (PAGES 2k Consortium, 2019; Schurer et al., 2014). The global-scale radiative forcing change appears thus to be responsible also for the multi-century cooling in West Antarctica. By contrast, higher frequency variations are controlled by regional processes as the correlation between the global mean and Antarctic temperature becomes very low for detrended time series.

Declaration of Competing Interest

The authors declare no competing interests.

Data availability

Data will be made available on request.

Acknowledgements

The resulting surface temperature reconstructions will be available when the manuscript is accepted. We thank Samantha Stevenson for her expertise on the outputs of iCESM1. HG is research director within the F.R.S.-FNRS (Belgium). Zhiqiang Lyu is supported by China Scholarship Council (CSC) – Université catholique de Louvain Co–Funding. QD is a Research Fellow within the F.R.S.-FNRS (Belgium). This work was partly supported by the Belgian Research Action through Interdisciplinary Networks (BRAIN-be) from Belgian Science Policy Office in the framework of the project "East Antarctic surface mass balance in the Anthropocene: observations and multiscale modelling (Mass2Ant)" (Contrat n° BR/165/A2/Mass2Ant). Computational resources have been provided by the supercomputing facilities of the Université catholique de Louvain (CISM/UCL) and the Consortium des Équipements de Calcul Intensif en Fédération Wallonie Bruxelles (CÉCI) funded by the Fond de la Recherche Scientifique de Belgique (F.R.S.–FNRS) under convention 2.5020.11.

Appendix A. Supplementary data

Supplementary data to this article can be found online at https://doi.org/10.1016/j.gloplacha.2023.104237.

References

Abram, N.J., McGregor, H.V., Tierney, J.E., Evans, M.N., McKay, N.P., Kaufman, D.S., 2016. Early onset of industrial-era warming across the oceans and continents. Nature 536 (7617), 411–418.

Allen, C.S., Weich, Z.C., 2022. Variety and distribution of diatom-based sea ice proxies in Antarctic marine sediments of the past 2000 years. Geosciences 12 (8), 282.

Banta, J.R., McConnell, J.R., Frey, M.M., Bales, R.C., Taylor, K., 2008. Spatial and temporal variability in snow accumulation at the West Antarctic ice sheet divide over recent centuries. J. Geophys. Res. Atmos. 113 (D23).

Barbara, L., Crosta, X., Leventer, A., Schmidt, S., Etourneau, J., Domack, E., Massé, G., 2016. Environmental responses of the Northeast Antarctic Peninsula to the Holocene climate variability. Paleoceanography 31 (1), 131–147.

Bárcena, M.A., Gersonde, R., Ledesma, S., Fabrés, J., Calafat, A.M., Canals, M., Flores, J. A., 1998. Record of Holocene glacial oscillations in Bransfield Basin as revealed by siliceous microfossil assemblages. Antarct. Sci. 10 (3), 269–285.

Bárcena, M.Á., Isla, E., Plaza, A., Flores, J.A., Sierro, F.J., Masqué, P., Palanques, A., 2002. Bioaccumulation record and paleoclimatic significance in the Western Bransfield Strait. The last 2000 years. Deep-Sea Res. II Top. Stud. Oceanogr. 49 (4–5), 935–950.

Bertler, N.A., Conway, H., Dahl-Jensen, D., Emanuelsson, D.B., Winstrup, M., Vallelonga, P.T., Zhang, X., 2018. The ross sea dipole-temperature, snow accumulation and sea ice variability in the Ross Sea region, Antarctica, over the past 2700 years. Clim. Past 14 (2), 193–214.

Bradley, R.S., Hughes, M.K., Diaz, H.F., 2003. Climate in medieval time. Science 302 (5644), 404–405.

Brady, E., Stevenson, S., Bailey, D., Liu, Z., Noone, D., Nusbaumer, J., Zhu, J., 2019. The connected isotopic water cycle in the Community Earth System Model version 1. J. Adv. Model. Earth Syst. 11 (8), 2547–2566.

Campagne, P., Crosta, X., Schmidt, S., Noëlle Houssais, M., Ther, O., Massé, G., 2016. Sedimentary response to sea ice and atmospheric variability over the instrumental period off Adélie Land, East Antarctica. Biogeosciences 13 (14), 4205–4218.

Caniupán, M., Lamy, F., Lange, C.B., Kaiser, J., Kilian, R., Arz, H.W., Tiedemann, R., 2014. Holocene sea-surface temperature variability in the Chilean fjord region. Quat. Res. 82 (2), 342–353.

Christ, A.J., Talaia-Murray, M., Elking, N., Domack, E.W., Leventer, A., Lavoie, C., LARISSA Group, 2015. Late Holocene glacial advance and ice shelf growth in Barilari Bay, Graham Land, West Antarctic Peninsula. Bulletin 127 (1–2), 297–315.

Clem, K.R., Fogt, R.L., Turner, J., Lintner, B.R., Marshall, G.J., Miller, J.R., Renwick, J.A., 2020. Record warming at the South Pole during the past three decades. Nat. Clim. Chang. 10 (8), 762–770.

Collins, J.A., Lamy, F., Kaiser, J., Ruggieri, N., Henkel, S., De Pol-Holz, R., Arz, H.W., 2019. Centennial-scale SE Pacific Sea surface temperature variability over the past 2,300 years. Paleoceanogr. Paleoclimatol. 34 (3), 336–352.

Crosta, X., Etourneau, J., Orme, L.C., Dalaiden, Q., Campagne, P., Swingedouw, D., Ikehara, M., 2021. Multi-decadal trends in Antarctic Sea-ice extent driven by ENSO-SAM over the last 2,000 years. Nat. Geosci. 14 (3), 156–160.

Dalaiden, Q., Goosse, H., Klein, F., Lenaerts, J., Holloway, M., Sime, L., Thomas, E.R., 2020. How useful is snow accumulation in reconstructing surface air temperature in Antarctica? A study combining ice core records and climate models. Cryosphere 14 (4), 1187–1207.

Dalaiden, Q., Goosse, H., Rezsöhazy, J., Thomas, E.R., 2021. Reconstructing atmospheric circulation and sea-ice extent in the West Antarctic over the past 200 years using data assimilation. Clim. Dyn. 57 (11), 3479–3503.

Ding, Q., Steig, E.J., Battisti, D.S., Küttel, M., 2011. Winter warming in West Antarctica caused by central tropical Pacific warming. Nat. Geosci. 4 (6), 398–403.

Dubinkina, S., Goosse, H., Sallaz-Damaz, Y., Crespin, E., Crucifix, M., 2011. Testing a particle filter to reconstruct climate changes over the past centuries. Int. J. Bifurcat. Chaos 21 (12), 3611–3618.

Etourneau, J., Collins, L.G., Willmott, V., Kim, J.H., Barbara, L., Leventer, A., Massé, G., 2013. Holocene climate variations in the western Antarctic Peninsula: evidence for sea ice extent predominantly controlled by changes in insolation and ENSO variability. Clim. Past 9 (4), 1431–1446.

Ferreira, D., Marshall, J., Bitz, C.M., Solomon, S., Plumb, A., 2015. Antarctic Ocean and sea ice response to ozone depletion: a two-time-scale problem. J. Clim. 28 (3), 1206–1226.

Fogt, R.L., Wovrosh, A.J., Langen, R.A., Simmonds, I., 2012. The characteristic variability and connection to the underlying synoptic activity of the Amundsen-Bellingshausen Seas Low. J. Geophys. Res. Atmos. 117 (D7).

Franzke, C.L., Barbosa, S., Blender, R., Fredriksen, H.B., Laepple, T., Lambert, F., Yuan, N., 2020. The structure of climate variability across scales. Rev. Geophys. 58 (2) e2019RG000657.

Gong, D., Wang, S., 1999. Definition of Antarctic oscillation index. Geophys. Res. Lett. 26 (4), 459–462.

Goosse, H., Braida, M., Crosta, X., Mairesse, A., Masson-Delmotte, V., Mathiot, P., Verleyen, E., 2012. Antarctic temperature changes during the last millennium: evaluation of simulations and reconstructions. Quat. Sci. Rev. 55, 75–90.

Goosse, H., Kay, J.E., Armour, K.C., Bodas-Salcedo, A., Chepfer, H., Docquier, D., Vancoppenolle, M., 2018. Quantifying climate feedbacks in polar regions. Nat. Commun. 9 (1), 1919.

Haddam, N.A., Siani, G., Michel, E., Kaiser, J., Lamy, F., Duchamp-Alphonse, S., Kissel, C., 2018. Changes in latitudinal sea surface temperature gradients along the Southern Chilean margin since the last glacial. Quat. Sci. Rev. 194, 62–76.

Hakim, G.J., Emile-Geay, J., Steig, E.J., Noone, D., Anderson, D.M., Tardif, R., Perkins, W.A., 2016. The last millennium climate reanalysis project: framework and first results. J. Geophys. Res. Atmos. 121 (12), 6745–6764.

Hosking, J.S., Orr, A., Marshall, G.J., Turner, J., Phillips, T., 2013. The influence of the Amundsen-Bellingshausen Seas low on the climate of West Antarctica and its representation in coupled climate model simulations. J. Clim. 26 (17), 6633–6648.

Jones, J.M., Gille, S.T., Goosse, H., Abram, N.J., Canziani, P.O., Charman, D.J., Vance, T. R., 2016. Assessing recent trends in high-latitude Southern Hemisphere surface climate. Nat. Clim. Chang. 6 (10), 917–926.

Jones, M.E., Bromwich, D.H., Nicolas, J.P., Carrasco, J., Plavcová, E., Zou, X., Wang, S. H., 2019. Sixty years of widespread warming in the southern middle and high latitudes (1957-2016). J. Clim. 32 (20), 6875–6898.

Klein, F., Abram, N.J., Curran, M.A., Goosse, H., Goursaud, S., Masson-Delmotte, V., Werner, M., 2019. Assessing the robustness of Antarctic temperature reconstructions over the past 2 millennia using pseudoproxy and data assimilation experiments. Clim. Past 15 (2), 661–684.

Kunz, T., Laepple, T., 2021. Frequency-dependent estimation of effective spatial degrees of freedom. J. Clim. 34 (18), 7373–7388.

Lamy, F., Rühlemann, C., Hebbeln, D., Wefer, G., 2002. High-and low-latitude climate control on the position of the southern Peru-Chile current during the Holocene. Paleoceanography 17 (2), 1–16.

Li, X., Cai, W., Meehl, G.A., Chen, D., Yuan, X., Raphael, M., Song, C., 2021. Tropical teleconnection impacts on Antarctic climate changes. Nat. Rev. Earth Environ. 2 (10), 680–698.

Lüning, S., Gałka, M., Vahrenholt, F., 2019. The medieval climate anomaly in Antarctica. Palaeogeogr. Palaeoclimatol. Palaeoecol. 532, 109251.

Lyu, Z., Goosse, H., Dalaiden, Q., Klein, F., Shi, F., Wagner, S., Braconnot, P., 2021. Spatial patterns of multi–centennial surface air temperature trends in Antarctica over 1–1000 CE: insights from ice core records and modeling. Quat. Sci. Rev. 271, 107205.

Manabe, S., Wetherald, R.T., 1975. The effects of doubling the CO^2 concentration on the climate of a general circulation model. J. Atmos. Sci. 32 (1), 3–15.

Mann, M.E., Zhang, Z., Rutherford, S., Bradley, R.S., Hughes, M.K., Shindell, D., Ni, F., 2009. Global signatures and dynamical origins of the little ice age and medieval climate anomaly. Science 326 (5957), 1256–1260.

Marshall, G.J., Stott, P.A., Turner, J., Connolley, W.M., King, J.C., Lachlan-Cope, T.A., 2004. Causes of exceptional atmospheric circulation changes in the Southern Hemisphere. Geophys. Res. Lett. 31 (14).

McGregor, H.V., Evans, M.N., Goosse, H., Leduc, G., Martrat, B., Addison, J.A., Ersek, V., 2015. Robust global ocean cooling trend for the pre-industrial Common Era. Nat. Geosci. 8 (9), 671–677.

Medley, B., Thomas, E.R., 2019. Increased snowfall over the Antarctic Ice Sheet mitigated twentieth-century sea-level rise. Nat. Clim. Chang. 9 (1), 34–39.

Mezgec, K., Stenni, B., Crosta, X., Masson-Delmotte, V., Baroni, C., Braida, M., Frezzotti, M., 2017. Holocene Sea ice variability driven by wind and polynya efficiency in the Ross Sea. Nat. Commun. 8 (1), 1–12.

Mulvaney, R., Abram, N.J., Hindmarsh, R.C., Arrowsmith, C., Fleet, L., Triest, J., Foord, S., 2012. Recent Antarctic Peninsula warming relative to Holocene climate and ice-shelf history. Nature 489 (7414), 141–144.

Neukom, R., Barboza, L.A., Erb, M.P., Shi, F., Emile-Geay, J., Evans, M.N., von Gunten, L., 2019a. Consistent multi-decadal variability in global temperature reconstructions and simulations over the Common Era. Nat. Geosci. 12 (8), 643.

Neukom, R., Steiger, N., Gómez-Navarro, J.J., Wang, J., Werner, J.P., 2019b. No evidence for globally coherent warm and cold periods over the preindustrial Common Era. Nature 571 (7766), 550–554.

O'Connor, G.K., Steig, E.J., Hakim, G.J., 2021. Strengthening Southern Hemisphere Westerlies and Amundsen sea low deepening over the 20th century revealed by proxy-data assimilation. Geophys. Res. Lett. 48 (24) e2021GL095999.

Orsi, A.J., Cornuelle, B.D., Severinghaus, J.P., 2012. Little Ice Age cold interval in West Antarctica: evidence from borehole temperature at the West Antarctic Ice Sheet (WAIS) divide. Geophys. Res. Lett. 39 (9).

Otto-Bliesner, B.L., Joussaume, S., Braconnot, P., Harrison, S.P., Abe-Ouchi, A., 2009. Modeling and Data Syntheses of Past Climates: Paleoclimate Modelling Intercomparison Project Phase II Workshop; Estes Park, Colorado, 15–19 September 2008.

Otto-Bliesner, B.L., Brady, E.C., Fasullo, J., Jahn, A., Landrum, L., Stevenson, S., Strand, G., 2016. Climate variability and change since 850 CE: an ensemble approach with the Community Earth System Model. Bull. Am. Meteorol. Soc. 97 (5), 735–754.

PAGES 2k Consortium, 2013. Continental-scale temperature variability during the past two millennia. Nat. Geosci. 6, 339–346.

PAGES 2k Consortium, 2019. Consistent multidecadal variability in global temperature reconstructions and simulations over the Common Era. Nat. Geosci. 12, 643–649.

PAGES 2k-PMIP3 group, 2015. Continental-scale temperature variability in PMIP3 simulations and regional temperature reconstructions over the past millennium. Clim. Past 11, 1673–1699.

Parkinson, C.L., 2019. A 40-y record reveals gradual Antarctic Sea ice increases followed by decreases at rates far exceeding the rates seen in the Arctic. Proc. Natl. Acad. Sci. 116 (29), 14414–14423.

Phipps, S.J., McGregor, H.V., Gergis, J., Gallant, A.J., Neukom, R., Stevenson, S., Van Ommen, T.D., 2013. Paleoclimate data–model comparison and the role of climate forcings over the past 1500 years. J. Clim. 26 (18), 6915–6936.

Pithan, F., Mauritsen, T., 2014. Arctic amplification dominated by temperature feedbacks in contemporary climate models. Nat. Geosci. 7 (3), 181–184.

Raphael, M.N., Holland, M.M., Landrum, L., Hobbs, W.R., 2019. Links between the Amundsen Sea low and sea ice in the Ross Sea: seasonal and interannual relationships. Clim. Dyn. 52 (3), 2333–2349.

Rowell, I., Mulvaney, R., Wolff, E., Pryer, H., Tetzner, D., Thomas, L., Martin, C., 2022. 1000 Years of Climate History from a Coastal West Antarctic Ice Core Site (No. EGU22-5914). Copernicus Meetings.

Schurer, A.P., Tett, S.F., Hegerl, G.C., 2014. Small influence of solar variability on climate over the past millennium. Nat. Geosci. 7 (2), 104–108.

Shevenell, A.E., Ingalls, A.E., Domack, E.W., Kelly, C., 2011. Holocene Southern Ocean surface temperature variability west of the Antarctic Peninsula. Nature 470 (7333), 250–254.

Silvestri, G., Berman, A.L., De Vleeschouwer, F., Wainer, I., 2021. Last millennium climate changes over the Antarctic Peninsula and southern Patagonia in CESM-LME simulations: differences between medieval climate anomaly and present-day temperatures. Quat. Sci. Rev. 274, 107273.

Simms, A.R., Bentley, M.J., Simkins, L.M., Zurbuchen, J., Reynolds, L.C., DeWitt, R., Thomas, E.R., 2021. Evidence for a "Little Ice Age" glacial advance within the Antarctic Peninsula–examples from glacially-overrun raised beaches. Quat. Sci. Rev. 271, 107195.

Steig, E.J., Morse, D.L., Waddington, E.D., Stuiver, M., Grootes, P.M., Mayewski, P.A., Whitlow, S.I., 2000. Wisconsinan and Holocene climate history from an ice core at Taylor Dome, western Ross Embayment, Antarctica. Geogr. Ann. Ser. B 82 (2–3), 213–235.

Steig, E.J., Schneider, D.P., Rutherford, S.D., Mann, M.E., Comiso, J.C., Shindell, D.T., 2009. Warming of the Antarctic ice-sheet surface since the 1957 international geophysical year. Nature 457 (7228), 459–462.

Steig, E.J., Ding, Q., White, J.W., Küttel, M., Rupper, S.B., Neumann, T.A., Korotkikh, E., 2013. Recent climate and ice-sheet changes in West Antarctica compared with the past 2,000 years. Nat. Geosci. 6 (5), 372–375.

Steiger, N., Hakim, G., 2016. Multi-timescale data assimilation for atmosphere–ocean state estimates. Clim. Past 12 (6), 1375–1388.

Steiger, N.J., Smerdon, J.E., Cook, E.R., Cook, B.I., 2018. A reconstruction of global hydroclimate and dynamical variables over the Common Era. Sci. Data 5 (1), 1–15.

Stenni, B., Buiron, D., Frezzotti, M., Albani, S., Barbante, C., Bard, E., Udisti, R., 2011. Expression of the bipolar see-saw in Antarctic climate records during the last deglaciation. Nat. Geosci. 4 (1), 46–49.

Stenni, B., Curran, M.A., Abram, N.J., Orsi, A., Goursaud, S., Masson-Delmotte, V., Frezzotti, M., 2017. Antarctic climate variability on regional and continental scales over the last 2000 years. Clim. Past 13 (11), 1609–1634.

Stevenson, S., Otto-Bliesner, B.L., Brady, E.C., Nusbaumer, J., Tabor, C., Tomas, R., Liu, Z., 2019. Volcanic eruption signatures in the isotope-enabled last millennium ensemble. Paleoceanogr. Paleoclimatol. 34 (8), 1534–1552.

Tardif, R., Hakim, G.J., Snyder, C., 2014. Coupled atmosphere–ocean data assimilation experiments with a low-order climate model. Clim. Dyn. 43 (5), 1631–1643.

Tardif, R., Hakim, G.J., Snyder, C., 2015. Coupled atmosphere–ocean data assimilation experiments with a low-order model and CMIP5 model data. Clim. Dyn. 45 (5), 1415–1427.

Tardif, R., Hakim, G.J., Perkins, W.A., Horlick, K.A., Erb, M.P., Emile-Geay, J., Noone, D., 2019. Last millennium reanalysis with an expanded proxy database and seasonal proxy modeling. Clim. Past 15 (4), 1251–1273.

Taylor, K.E., Stouffer, R.J., Meehl, G.A., 2012. An overview of CMIP5 and the experiment design. Bull. Am. Meteorol. Soc. 93 (4), 485–498.

Thomas, E.R., Van Wessem, J.M., Roberts, J., Isaksson, E., Schlosser, E., Fudge, T.J., Ekaykin, A.A., 2017. Regional Antarctic snow accumulation over the past 1000 years. Clim. Past 13 (11), 1491–1513.

Thompson, D.W., Solomon, S., 2002. Interpretation of recent Southern Hemisphere climate change. Science 296 (5569), 895–899.

Tierney, J.E., Tingley, M.P., 2018. BAYSPLINE: a new calibration for the alkenone paleothermometer. Paleoceanogr. Paleoclimatol. 33 (3), 281–301.

Turner, J., Lu, H., White, I., King, J.C., Phillips, T., Hosking, J.S., Deb, P., 2016. Absence of 21st century warming on Antarctic Peninsula consistent with natural variability. Nature 535 (7612), 411–415.

Turner, J., Marshall, G.J., Clem, K., Colwell, S., Phillips, T., Lu, H., 2020. Antarctic temperature variability and change from station data. Int. J. Climatol. 40 (6), 2986–3007.

Van Wessem, J.M., Van De Berg, W.J., Noël, B.P., Van Meijgaard, E., Amory, C., Birnbaum, G., Van Den Broeke, M.R., 2018. Modelling the climate and surface mass balance of polar ice sheets using RACMO2–part 2: Antarctica (1979–2016). Cryosphere 12 (4), 1479–1498.

Vorrath, M.E., Müller, J., Rebolledo, L., Cárdenas, P., Shi, X., Esper, O., Mollenhauer, G., 2020. Sea ice dynamics in the Bransfield Strait, Antarctic Peninsula, during the past 240 years: a multi-proxy intercomparison study. Clim. Past 16 (6), 2459–2483.

Winstrup, M., Vallelonga, P., Kjær, H.A., Fudge, T.J., Lee, J.E., Riis, M.H., Wheatley, S., 2019. A 2700-year annual timescale and accumulation history for an ice core from Roosevelt Island, West Antarctica. Clim. Past 15 (2), 751–779.